

ARTICLE

PPAR γ is essential for the development of bone marrow erythroblastic island macrophages and splenic red pulp macrophages

Katarzyna Okreglicka¹, Irina Iten¹, Lea Pohlmeier¹, Lucas Onder², Qian Feng¹, Michael Kurrer³, Burkhard Ludewig², Peter Nielsen¹, Christoph Schneider^{1,4}, and Manfred Kopf¹

Tissue-resident macrophages play a crucial role in maintaining homeostasis. Macrophage progenitors migrate to tissues perinatally, where environmental cues shape their identity and unique functions. Here, we show that the absence of PPAR γ affects neonatal development and VCAM-1 expression of splenic iron-recycling red pulp macrophages (RPMs) and bone marrow erythroblastic island macrophages (EIMs). Transcriptome analysis of the few remaining *Pparg*-deficient RPM-like and EIM-like cells suggests that PPAR γ is required for RPM and EIM identity, cell cycling, migration, and localization, but not function in mature RPMs. Notably, *Spi-C*, another transcription factor implicated in RPM development, was not essential for neonatal expansion of RPMs, even though the transcriptome of *Spic*-deficient RPMs was strongly affected and indicated a loss of identity. Similarities shared by *Pparg*- and *Spic*-deficient RPM-like cells allowed us to identify pathways that rely on both factors. PPAR γ and *Spi-C* collaborate in inducing transcriptional changes, including VCAM-1 and integrin α_D expression, which could be required for progenitor retention in the tissue, allowing access to niche-related signals that finalize differentiation.

Introduction

Tissue-resident macrophages are immune phagocytes present in almost all tissues (Hume and Gordon, 1983; Hume et al., 1983; Lee et al., 1985). In addition to general functions, like pathogen clearance and tissue homeostasis (for a review, refer to Gordon, 2007, and Murray and Wynn, 2011), tissue-resident macrophages are specialized to perform additional environment-imposed functions (Chow et al., 2011; Parkhurst et al., 2013). The mechanisms underlying this adaptation to the tissue's needs are poorly understood. Tissue macrophages develop from fetal progenitors and are able to homeostatically self-renew in adulthood (Ginhoux et al., 2010; Hashimoto et al., 2013; Jakubzick et al., 2013; Schulz et al., 2012; Yona et al., 2013). Upon tissue seeding, which occurs before birth, progenitor cells receive environment-specific signals, such as cytokines or metabolites, which induce signaling cascades and a unique differentiation program, leading to the development of specialized macrophages (Amit et al., 2016; Gautier et al., 2012b; Glass and Natoli, 2016; Gosselin et al., 2014; Lavin et al., 2015; Lavin et al., 2014). PU.1—encoded by the *Sp1* gene and a member of the ETS domain-containing family—has been shown to be an essential transcription factor for macrophage development

(Schulz et al., 2012). It binds to both common and subset-specific genomic locations and is required for collaborative interactions with alternative sets of transcription factors induced by environmental triggers in each tissue-specific macrophage subset (Gosselin et al., 2014).

While fate mapping studies have helped to understand the origin of macrophages, transcriptome and enhancer region analyses have provided crucial information about tissue-specific gene signatures (Gautier et al., 2012b; Gomez Perdiguero et al., 2015; Gosselin et al., 2014; Hoeffel et al., 2015; Lavin et al., 2014). For example, TGF β -induced SMAD2/3 activation is crucial for microglia development (Abutbul et al., 2012; Butovsky et al., 2014), while peritoneal macrophages depend on GATA6, which is induced by retinoic acid binding to the retinoic acid receptor- β (Okabe and Medzhitov, 2014). Terminal differentiation of osteoclasts, a macrophage subset residing in bones and responsible for bone resorption, depends on NFATc1 activation via receptor activator of NF- κ B ligand signaling (Takayanagi et al., 2002). In lungs, GM-CSF production by lung epithelial cells induces peroxisome proliferator-activated receptor- γ (PPAR γ), which is indispensable for alveolar macrophage (AM) differentiation

¹Institute of Molecular Health Sciences, Swiss Federal Institute of Technology, Zurich, Switzerland; ²Institute of Immunobiology, Cantonal Hospital, St. Gallen, Switzerland; ³Pathology praxis, Zurich, Switzerland; ⁴Institute of Physiology, University of Zurich, Zurich, Switzerland.

Correspondence to Manfred Kopf: manfred.kopf@ethz.ch.

© 2021 Okreglicka et al. This article is distributed under the terms of an Attribution–Noncommercial–Share Alike–No Mirror Sites license for the first six months after the publication date (see <http://www.rupress.org/terms/>). After six months it is available under a Creative Commons License (Attribution–Noncommercial–Share Alike 4.0 International license, as described at <https://creativecommons.org/licenses/by-nc-sa/4.0/>).

from fetal monocytes (Guilliams et al., 2013; Schneider et al., 2014). The spleen contains several macrophage subsets, including marginal zone macrophages, marginal metallophilic macrophages (MMMs), and red pulp macrophages (RPMs). Marginal zone macrophages and MMMs have been shown to be dependent on nuclear liver X receptor- α , which is activated by a so-far-unknown trigger (A-Gonzalez et al., 2013). RPMs develop in an M-CSF-dependent manner and rely on Spi-C, a PU.1-related factor (Kohyama et al., 2009; Kurotaki et al., 2011). Similarly, Spi-C is needed for a population of vascular cell adhesion molecule-1 (VCAM-1)-positive bone marrow macrophages (Haldar et al., 2014), also known as bone marrow erythroblastic island macrophages (EIMs) due to their function in facilitating iron recycling from senescent RBCs, similar to RPMs in the spleen (Kurotaki et al., 2015). Both RPMs and EIMs constitutively degrade hemoglobin and metabolize the highly oxidative intermediate product of this degradation, heme. The BTB domain and CNC homologue 1 (Bach1) transcription regulator represses Spi-C expression in monocytes. It has been shown that heme can bind to Bach1, and heme-bound Bach1 is marked for proteasomal degradation. This results in Spi-C activation and macrophage differentiation (Haldar et al., 2014).

In this study, we describe a previously unknown crucial role of PPAR γ in RPM and EIM development. Although this factor is the main driver of perinatal AM differentiation, the programs induced by PPAR γ in lungs and spleen are distinct and, in the latter case, are not related to lipid metabolism. Moreover, we show that upon tissue seeding, developing RPMs downregulate migration-related markers and strongly upregulate integrin α_D , which is uniquely expressed by this macrophage subset and is correlated with cell retention (Aziz et al., 2017). These results are an example of how niche-specific signals collaborate with the transcriptional regulator PPAR γ to promote alternative differentiation programs.

Results

Spi-C is not essential for neonatal RPM development

Spi-C is a signature transcription factor of RPMs, and adult *Spic*-deficient mice have been reported to lack RPMs and EIMs (Haldar et al., 2014). Since most resident macrophages develop perinatally from fetal precursors, we have revisited the role of Spi-C for RPMs and compared newborn *Spic*^{-/-} to WT counterparts. First, we confirmed a strong reduction of RPMs and EIMs in adult *Spic*^{-/-} mice (Figs. 1 A and S1 B). Strikingly, the number of RPMs and EIMs in 7-d-old mice were unaffected by the lack of Spi-C (Figs. 1 B and S1 C). At the age of 2 and 4 wk, RPM numbers were already significantly reduced (Fig. S1 D), although not as striking as in adults, indicating a loss of these populations after their neonatal expansion. The transcriptome analysis of RPM from 7-d-old pups showed that the expression of 1,447 genes in *Spic*-deficient RPMs was changed more than 2.8-fold (false discovery rate [FDR] < 0.05). The top 50 differentially expressed genes (DEGs) are listed in Fig. 1 C. Gene ontology (GO) analysis further identified the altered biological pathways in *Spic*-deficient cells, including decreased processes of oxidation reduction, cellular oxidant reduction or heme catabolism and

increased cell adhesion, signal transduction, or response to stimulus (Fig. 1 D). Moreover, comparison of DEGs ($|\log_2 \text{ratio}| > 1.5$) to signature genes, defined for different tissue-resident macrophage subsets by Lavin et al. (2014), revealed decreased expression of many RPM-related signature genes and increased expression of genes related to macrophages from other tissues, like colon or brain (Fig. 1 E). Previously described signature genes, like Spi-C, VCAM-1, and TREML4 (Haldar et al., 2014), present in the splenic macrophage signature identified by Lavin et al. (2014) were all significantly reduced (Fig. 1 F). Interestingly, we noted a significant decrease in PPAR γ mRNA (Fig. 1 F) and protein expression (Fig. 1, G and H; and Fig. S1 E) in *Spic*-deficient RPMs and EIMs, possibly indicating a role for PPAR γ in the development of iron-recycling macrophages, similar to its role in AMs (Schneider et al., 2014). These results show that in the absence of Spi-C, RPM- and EIM-like cells can be produced but they could be functionally altered and are not maintained after initial expansion.

Reduced EIMs and iron-recycling RPMs in the absence of PPAR γ

To assess whether PPAR γ is important for RPM development, we used a *Vav1-Cre/Pparg*^{fl/fl} mouse line that efficiently deletes PPAR γ in all hematopoietic cells, including differentiating fetal monocytes (Schneider et al., 2014). Development of RPMs and EIMs—characterized as F4/80⁺CD11b^{int}VCAM-1⁺ cells—is considerably impaired in adult *Vav1-Cre/Pparg*^{fl/fl} mice (Fig. 2, A and B). Notably, *Cd11c-Cre/Pparg*^{fl/fl} mice and *LysM-Cre/Pparg*^{fl/fl} mice showed no significant reduction of RPMs and EIMs (Fig. S2, A–C), most probably due to poor *CD11c* and *LysM* promoter-driven Cre recombinase expression and accordingly inefficient PPAR γ deletion in macrophages (Schneider et al., 2014). In contrast, *Vav1-Cre* expression in *Rosa26-RFP* reporter mice induced deletion of a loxP-flanked stop cassette and RFP expression in >95% of RPMs without Cre toxicity (Fig. S2 D). Immunohistology of spleens confirmed the almost complete absence of F4/80⁺ cells in the red pulp of *Vav1-Cre/Pparg*^{fl/fl} mice, while CD169⁺ (MOMA⁺) MMMs, localized at the interface of white pulp and red pulp, were unchanged from WT controls (Fig. 2 C). RPMs are critical for phagocytosis of senescent RBCs and iron recycling. Nevertheless, RBC number, mean corpuscular volume, hematocrit (HCT), hemoglobin, and reticulocyte counts were unaffected in the circulating blood of *Vav1-Cre/Pparg*^{fl/fl} mice (Fig. 2 D); however, consistent with the report for *Spic*-deficient mice, *Vav1-Cre/Pparg*^{fl/fl} mice accumulated ferric iron in the spleen (Fig. 2, E and F).

RPMs require PPAR γ intrinsically for neonatal development

Most tissue macrophages arise during perinatal development (Ginhoux and Guilliams, 2016). Indeed, we noted a 20-fold expansion of RPMs between days 2 and 5 (Fig. 3 A), concomitant with the increase in PPAR γ expression (Fig. 3 B). To assess whether PPAR γ regulates postnatal RPM development, we analyzed RPM populations in *Vav1-Cre/Pparg*^{fl/fl} mice and *Pparg*^{fl/fl} littermate controls at different days after birth. While the postnatal expansion of RPMs was strongly reduced in the absence of PPAR γ (Figs. 3 A and S3 A), this reduction did not

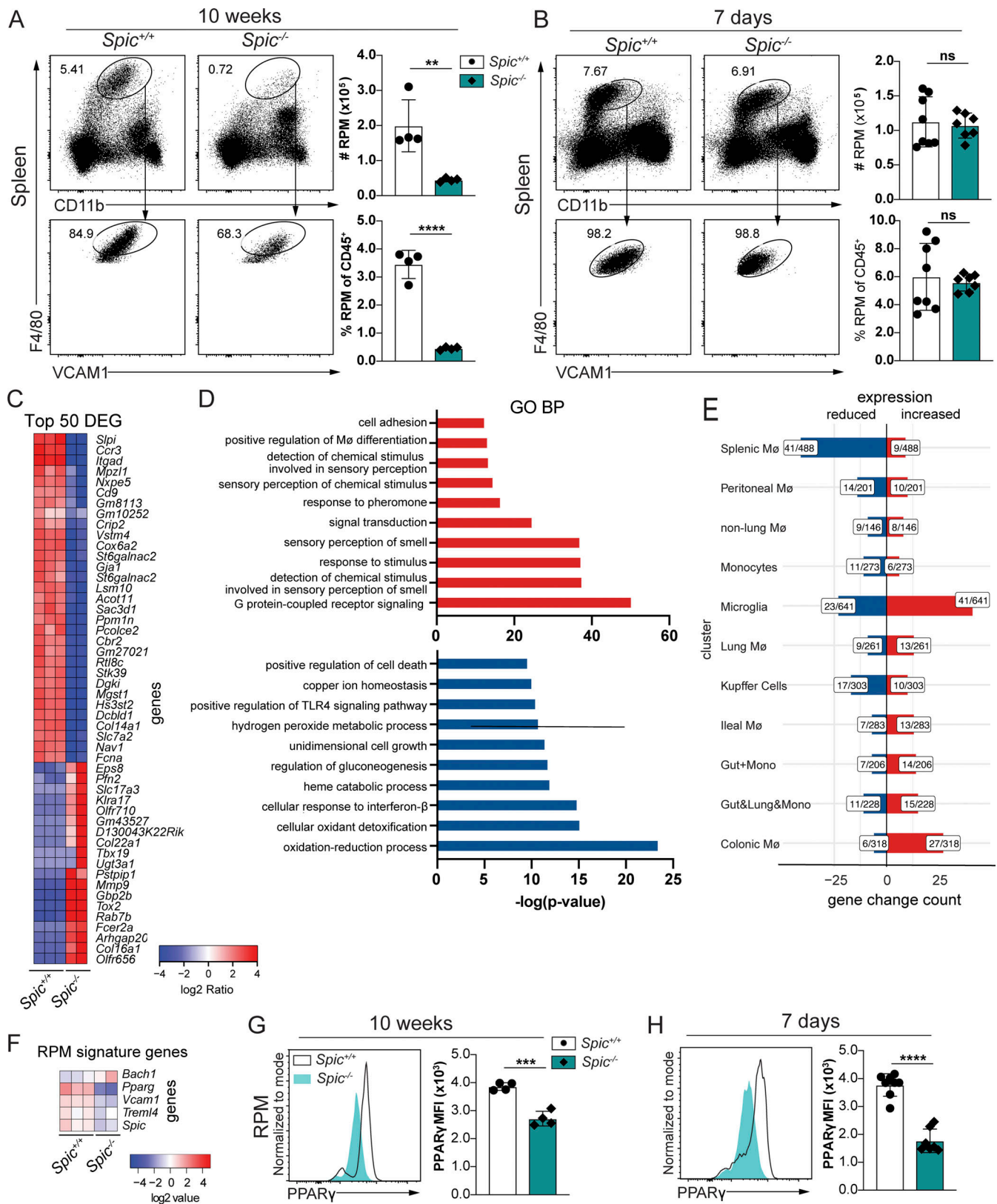


Figure 1. **RPM numbers in *Spic*^{-/-} mice are not affected early after birth.** (A and B) Flow cytometry of spleens from 10-wk-old (A) and 5–7-d-old (B) *Spic*^{+/+} and *Spic*^{-/-} mice; plots of a representative individual (left) and bar graphs (right) showing RPM counts (upper) and their frequencies of CD45⁺ cells (lower). RPMs were gated as shown in Fig. S1 A. (C) Heat map showing the top 50 DEGs between *Spic*^{+/+} and *Spic*^{-/-} RPMs (according to absolute values of *g*fold). Cells were isolated from 7-d-old mice. (D) Upregulated (red) and downregulated (blue) GO terms for Biological Process (BP) from comparison of *Spic*^{-/-} over *Spic*^{+/+} RPMs (*P* < 0.01). (E) Bar graphs showing upregulated (red) and downregulated (blue) genes from a comparison of *Spic*^{-/-} over *Spic*^{+/+} RPMs (log₂

ratio) > 1.5) with gene signatures of different tissue-resident macrophages (MΦ) and monocytes derived from Lavin et al. (2014). (F) Heat maps showing top RPM signature genes. (G and H) Histograms and MFI of PPARγ expression in RPMs derived from 10-wk-old (G) and 5–7-d-old (H) *Spic*^{-/-} and *Spic*^{+/-} mice. Data shown are from a single experiment (C–F) or pooled data from three independent experiments (A, B, G, and H); mean and SD from four to eight mice per group). **, P < 0.01; ***, P < 0.001; ****, P < 0.0001 (unpaired two-tailed Student's t test).

significantly affect the total number of splenocytes (Fig. S3 B). The frequency of Ly6C⁺ monocytes was increased in neonatal *Vav1-Cre/Pparg*^{fl/fl} mice and inversely corresponded to the

decrease in RPMs (Fig. S3, C and D). Moreover, the few remaining RPM-like cells in *Vav1-Cre/Pparg*^{fl/fl} neonates entered cell cycling, indicated by Ki67 expression, and proliferated

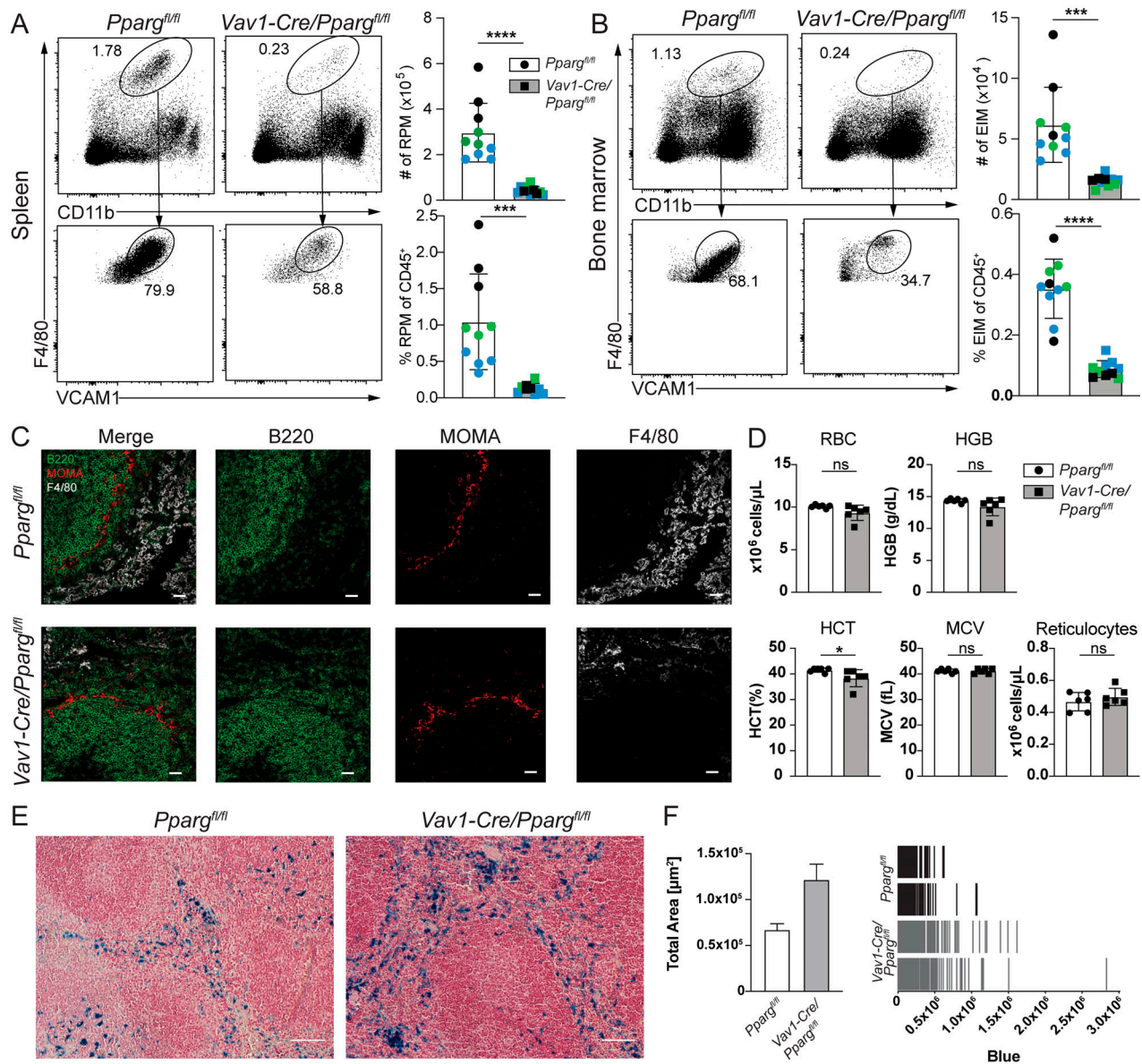


Figure 2. Development of iron-recycling macrophages is abrogated in the absence of PPARγ. (A and B) Flow cytometry plots of spleen (A) and bone marrow (B) from *Pparg*^{fl/fl} and *Vav1-Cre/Pparg*^{fl/fl} mice (7–11 wk old; pooled from three experiments indicated by different colors) and bar graphs showing RPM/EIM counts and their frequencies of CD45⁺ cells. RPMs/EIMs were pregated as live CD45⁺ cells. (C) Images of immunohistochemistry staining of B220 (B cell marker), MOMA (metallophilic macrophage marker), and F4/80 (RPM marker) on splenic sections. White scale bars, 25 μm. (D) Comparison of the numbers of RBCs and reticulocytes, hemoglobin (HGB), HCT, and mean corpuscular volume (MCV) of RBCs from blood test of *Pparg*^{fl/fl} and *Vav1-Cre/Pparg*^{fl/fl} mice. (E) Representative microscopic images of splenic sections demonstrating ferric iron deposits by Perls' Prussian Blue stain. White scale bars, 50 μm. (F) Bar graph (left) and rug plot (right) presenting the quantification of blue-stained area from two biological replicates. The presented data are pooled from three independent experiments (A and B; mean and SD of 10 mice per group) or are representative of two independent experiments (D; mean and SD of three to five mice per group). *, P < 0.05; ***, P < 0.001; ****, P < 0.0001 (unpaired two-tailed Student's t test).

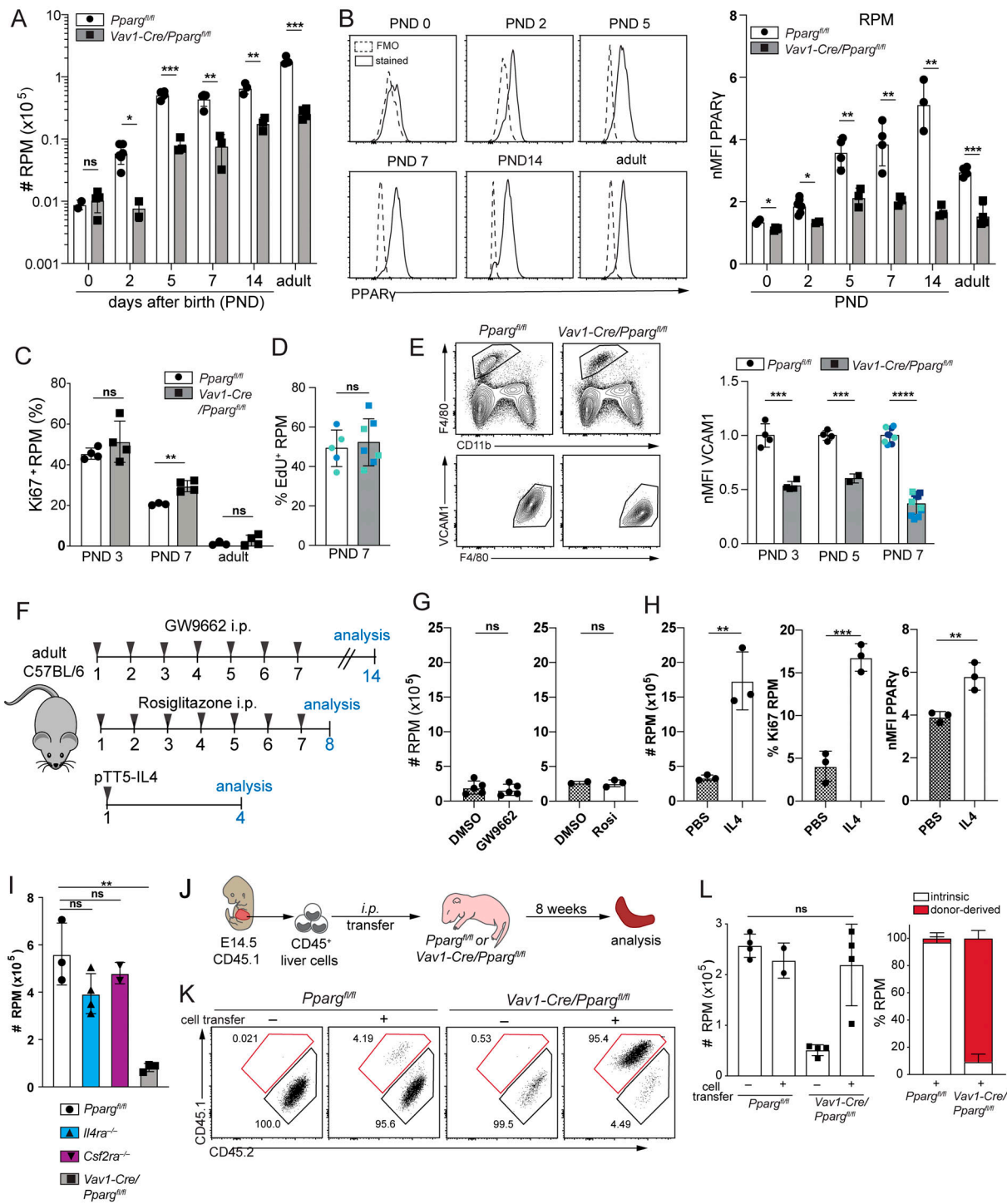


Figure 3. RPMs require PPAR γ intrinsically for their development. (A) Total RPM counts from *Pparg^{fl/fl}* and *Vav1-Cre/Pparg^{fl/fl}* mice (gated as shown in Fig. 2 A) at indicated days after birth (postnatal day [PND]). (B) PPAR γ expression by RPMs from representative WT (*Pparg^{fl/fl}*) mice at indicated PNDs and in adults shown as histograms (left) and as averages of MFI (normalized to FMO controls) from groups of WT and KO mice (right). (C and D) Bar graphs showing percentages of Ki67⁺ (C) and Edu⁺ (D) RPMs at indicated time points. (E) VCAM-1 expression gated on F4/80⁺ RPMs shown as dot plots from representative individuals at PND 7 (left) and bar graphs showing MFI (mean and SD) of groups of *Pparg^{fl/fl}* and *Vav1-Cre/Pparg^{fl/fl}* at PND 3, 5, and 7 (different color symbols indicate separate experiments; right). (F) Graphical scheme of experiments aiming at blocking (G) and inducing (H) PPAR γ expression. (G) Total RPM counts from adult C57BL/6 mice treated i.p. with 1 mg/kg of PPAR γ inhibitor GW9662 (left) or with 10 mg/kg of PPAR γ ligand rosiglitazone (right) for 7 consecutive days prior to analysis at days indicated in the scheme. (H) Total RPM counts, frequency of Ki67⁺, and normalized MFI of PPAR γ in RPMs from adult C57BL/6 mice at day 4 after hydrodynamic IL-4 gene delivery (plasmid pTT5-IL4). (I) Total RPM counts from mice of indicated genotypes. All mice were 8–12 wk old; RPMs gated as in Fig. 2 A. (J) Graphical presentation of experiments designed to test the fetal monocyte intrinsic requirement of PPAR γ for RPM development. CD45⁺ cells were sorted from fetal livers of E14.5 embryos (CD45.1) and subsequently transferred to *Pparg^{fl/fl}* and *Vav1-Cre/Pparg^{fl/fl}* newborns. Analysis of the RPM reconstitution was performed 8 wk after transfer. (K) Dot plots showing RPM origin in recipient mice 8 wk after transfer. RPMs are gated as live

CD11b^{int}F4/80⁺VCAM-1⁺CD11c^{lo}; red gates indicate CD45.1⁺ RPMs (derived from transferred fetal progenitors). (L) RPM counts of mice supplemented with fetal monocyte precursors or not (left), and frequencies of donor-derived and intrinsic RPMs in mice adoptively transferred with fetal precursors (right). The presented data are representative of at least two independent experiments, except C and H, which come from a single experiment. Symbols in column graphs represent values of individuals and the column size mean (\pm SD). *, $P < 0.05$; **, $P < 0.01$; ***, $P < 0.001$; ****, $P < 0.0001$ (unpaired two-tailed Student's *t* test).

comparable to WT littermate controls (Fig. 3, C and D). Interestingly, VCAM-1 expression, which is critical for RPM development (Ulyanova et al., 2016), was substantially reduced in *Pparg*-deficient RPMs during the first week after birth (Fig. 3 E). Although *Vav1-Cre/Pparg^{fl/fl}* mice lack PPAR γ in all hematopoietic cells, the numbers of B cells, T cells, dendritic cells (DCs), and other myeloid subsets in spleen and blood were not changed in adult mice (Fig. S3, E and F), in support of a specific direct role of PPAR γ for RPM differentiation.

Treatment of adult WT mice with the PPAR γ antagonist (GW9662) or agonist (rosiglitazone) for 7 consecutive days had no effect on RPM number or their phenotype (Fig. 3 G). As IL-4 has been previously described as a potent activator of PPAR γ expression in bone marrow-derived macrophages in vitro (Szanto et al., 2010), we tested its capability to induce PPAR γ in vivo. Overexpression of IL-4 by hydrodynamic gene delivery in WT mice led to an over fourfold increase in RPM number, an elevated frequency of Ki67⁺ RPMs, and higher PPAR γ mean fluorescence intensity (MFI) of RPM (Fig. 3 H). However, a complete deficiency of either IL-4 receptor or GM-CSF receptor (*Csf2ra*), which are known inducers of PPAR γ in M2 macrophages (Odegaard et al., 2007; Szanto et al., 2010) and AM (Bonfield et al., 2003; Schneider et al., 2014), respectively, did not cause any impairment of RPM development (Fig. 3 I).

The fetal liver contains progenitors with the capacity to give rise to multiple types of tissue macrophages (Epelman et al., 2014). To assess a cell-autonomous requirement of PPAR γ for RPM development, we sorted CD45⁺ cells from the fetal liver of E14.5 WT embryos (CD45.1) and injected them into newborn *Vav1-Cre/Pparg^{fl/fl}* and *Pparg^{fl/fl}* mice. 8 wk later, RPMs in *Vav1-Cre/Pparg^{fl/fl}* mice were completely restored with cells derived from transferred WT fetal precursors (Fig. 3, J-L). Notably, transferred cells did not contribute to macrophages in the liver (Fig. S3, G and H). Overall, our data demonstrate an intrinsic requirement for PPAR γ in the perinatal development of RPMs.

Impaired RPM development in the absence of PPAR γ affects removal of senescent RBCs and reticulocytosis after hemolytic anemia

Although RPMs and EIMs were drastically reduced in the absence of PPAR γ , we noted a small remaining population with comparable surface marker expression (Fig. 2, A and B). These *Vav1-Cre/Pparg^{fl/fl}*-derived RPMs did not differ morphologically from their WT counterparts (Fig. 4 A), other than the fact that the cell size seems to be increased. To better characterize the transcriptional program regulated by PPAR γ in RPMs and EIMs, we sorted the remaining F4/80^{hi}VCAM-1⁺ population from the spleen and bone marrow of 7-d-old *Vav1-Cre/Pparg^{fl/fl}* mice and compared their transcriptomes to *Pparg*-sufficient RPMs and EIMs from littermate controls using RNA sequencing. Principal component analysis (PCA) showed that the RPM and EIM

molecular signatures differed between the two genotypes (Fig. 4 B). 485 and 377 DEGs were detected for RPMs and EIMs, respectively (with threshold $|\log_2 \text{ratio}| > 1.5$; FDR < 0.05), with the top 50 DEGs shown in Fig. 4 C and Fig. S4 A. GO analysis identified altered biological processes in *Pparg*-deficient cells, showing that pathways like chemotaxis or inflammatory/immune response were activated, while DNA replication, erythrocyte development, and heme biosynthesis were the most significantly reduced processes (Figs. 4 D and S4 B) in both subsets when compared with WT RPMs and EIMs. As is the case for *Spic*-deficient RPMs, the loss of PPAR γ led to decreased expression of multiple RPM signature genes, while the expression of many genes from signatures of other tissue-resident macrophages was increased (Figs. 4 E and S4 C).

Vav1-Cre/Pparg^{fl/fl} mice have a decreased number of EIMs, which are nurse cells for erythroblasts and control the proper development of reticulocytes (Bessis, 1958; Chow et al., 2013; Chow et al., 2011). Upon hemolytic stress and anemia induced by phenylhydrazine treatment (Fig. 4 F), *Pparg*-deficient mice (>20 wk old) showed an impaired release of reticulocytes into the blood stream (Fig. 4 G), as has been reported for mice deprived of CD169⁺ macrophages (Chow et al., 2013); however, this difference was not observed in young *Pparg*-deficient mice (Fig. S4 G). Also, we did not observe a decrease in HCT for *Vav1-Cre/Pparg^{fl/fl}* mice (Figs. 4 H and S4 H). Notably, the overall disposal of senescent RBCs was strikingly reduced in *Vav1-Cre/Pparg^{fl/fl}* mice (Fig. 4, I and J), while *Pparg*-deficient RPMs possessed a comparable ability to phagocytose stressed RBC at the single cell level (Fig. 4 K; and Fig. S4, D-F). We propose that the strongly reduced number of RPMs in *Vav1-Cre/Pparg^{fl/fl}* mice is the reason RBCs are cleared less efficiently. Moreover, Kupffer cells (KCs), which should help in degrading damaged RBCs, were not more active in *Vav1-Cre/Pparg^{fl/fl}* mice (Figs. 4 K and S4 E); thus, it appears that a small number of RPM-like cells with the ability to phagocytose RBCs can develop independently of PPAR γ , but this is not sufficient to allow for an efficient clearance of senescent RBCs and the reuse of iron.

PPAR γ maintains RPM identity throughout life

Although PCA analysis showed that the transcriptomes of *Spic*- and *Pparg*-deficient RPMs differed significantly (Fig. 5 A), around 50 genes were commonly down- and upregulated for both KOs (Fig. 5 B; threshold $|\log_2 \text{ratio}| > 1.5$). *C5ar1*, *Pf4*, and *Tox2* belong to the top three commonly upregulated genes, while *Itgad*, *Vstm4*, and *Mrap* include the top three commonly down-regulated genes. Consistently, C5aR1 (CD88) surface levels were strikingly upregulated on RPMs and EIMs in the absence *Pparg* and *Spic* (Fig. 5, C and D). We next crossed *Ubc-CreERT2*, hereafter referred to as *CreERT2*, with *Pparg^{fl/fl}* mice to generate *CreERT2/Pparg^{fl/fl}* mice, allowing temporally controlled deletion of PPAR γ . Tamoxifen treatment of adults resulted in the excision

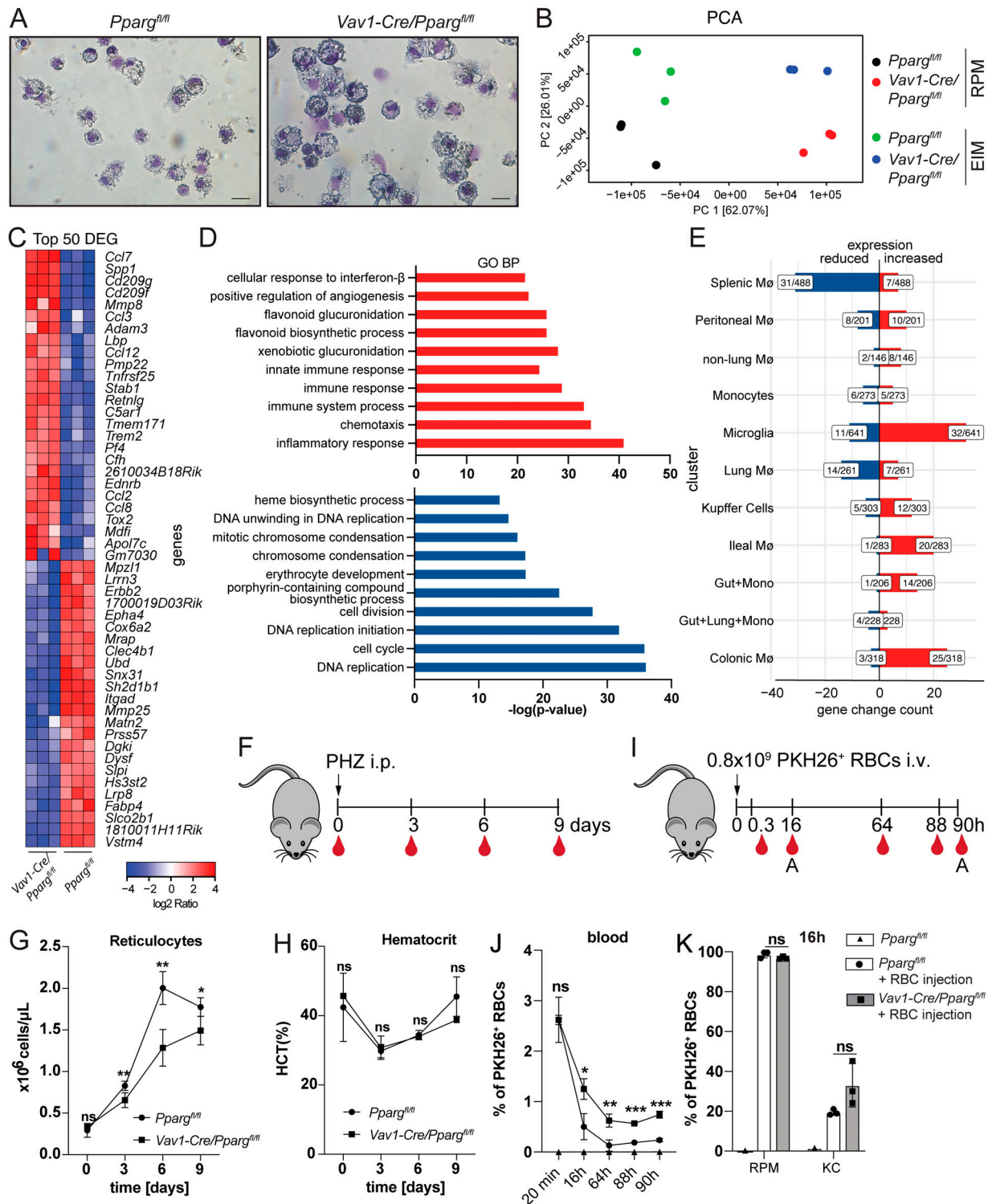


Figure 4. **PPAR γ is not essential for iron metabolism and removal of senescent RBCs by RPMs.** (A) Cytopsin of sorted RPMs derived from adult *Pparg^{fl/fl}* and *Vav1-Cre/Pparg^{fl/fl}* mice. Black scale bars, 20 μ M. (B) PCA performed on transcriptome from three biological replicates from *Pparg^{fl/fl}* RPM (black dots), *Vav1-Cre/Pparg^{fl/fl}* RPM (red dots), *Pparg^{fl/fl}* EIM (green dots), and *Vav1-Cre/Pparg^{fl/fl}* EIMs (blue dots). (C) Heat map showing top 50 DEGs between *Pparg^{fl/fl}* and *Vav1-Cre/Pparg^{fl/fl}* RPMs (according to absolute values of *gfold*). Cells were isolated from 7-d-old mice. (D) Upregulated (red) and downregulated (blue) GO terms for Biological Process (BP) from comparison of *Vav1-Cre/Pparg^{fl/fl}* over *Pparg^{fl/fl}* RPMs ($P < 0.01$). (E) Bar graphs showing upregulated (red) and downregulated (blue) genes from a comparison of *Vav1-Cre/Pparg^{fl/fl}* over *Pparg^{fl/fl}* RPMs ($|\log_2 \text{ratio}| > 1.5$) with gene signatures of different tissue-resident macrophages (M Φ) and monocytes derived from Lavin et al. (2014). (F) Graphical presentation of the experiment where hemolytic anemia was induced in *Pparg^{fl/fl}* and *Vav1-Cre/Pparg^{fl/fl}* mice (22–25 wk old); phenylhydrazine (PHZ; 30 mg/kg) was i.v. injected and blood samples were collected on indicated days. (G and H) Blood reticulocyte number (G) and HCT (H) was measured at indicated days. (I) Graphical presentation of the experiment where PKH26-labeled stressed RBCs were i.v. injected into *Pparg^{fl/fl}* and *Vav1-Cre/Pparg^{fl/fl}* mice (12–16 wk old); RBCs were stressed and labeled with the dye before injections and

their clearance from the bloodstream was assessed at the indicated time points. **(J and K)** Frequencies of PKH26-positive RBCs in the blood (J) and frequencies of RBC-PKH26-positive RPMs and KCs (K), illustrating their phagocytosing capacities 16 h after injection. The presented data are from a single experiment with three mice per group (A–G) or are representative of two independent experiments (F–K); mean and SD from three to five mice per group). *, $P < 0.05$; **, $P < 0.01$; ***, $P < 0.001$ (unpaired two-tailed Student's *t* test).

of floxed *Pparg* alleles and absence of PPAR γ protein only in a fraction of RPMs and EIMs that can be separated from PPAR γ -expressing cells by CD88 expression (Figs. 5 E and S5 A). Indeed, CD88^{hi} cells were observed only in tamoxifen-treated *CreERT2/Pparg*^{fl/fl} mice, which confirms results obtained in *Vav1-Cre/Pparg*^{fl/fl} mice (Fig. 5, F and G) and suggests that PPAR γ potentially suppresses CD88 expression. Interestingly, absence of PPAR γ did not affect RPM and EIM numbers 2.5 wk after the first tamoxifen treatment (Fig. 5 H), indicating that PPAR γ is not required for their survival at steady state. Nonetheless, deletion of PPAR γ in adult RPMs (i.e., sorted CD88^{hi} RPMs) resulted in downregulation of 125 genes and upregulation of only 13 genes ($|\log_2 \text{ratio}| > 1.5$; FDR < 0.05). The top 50 DEGs are listed in Fig. 5 I. Similar to *Pparg*-deficient RPMs and EIMs from young mice, GO analysis identified biological processes, like immune response and chemotaxis, as increased in tamoxifen-treated *CreERT2/Pparg*^{fl/fl} cells (Fig. 5 J). However, the top pathways decreased in the previous comparisons in *Vav1-Cre/Pparg*^{fl/fl} mice did not change significantly in *CreERT2/Pparg*^{fl/fl} cells, and there were few changes in the expression macrophage signature genes associated with different tissue macrophage subsets (Fig. 5, J and K).

Taken together, these results suggest that PPAR γ plays a pivotal role in proper localization and maturation of RPMs and EIMs, while its function in their maintenance at steady state is less critical.

Common transcriptional changes associated with *Pparg* and *Spic* deficiency in RPMs

The dependence of RPM development on PPAR γ is reminiscent of the phenotype detected in adult *Spic*^{-/-} mice. Given the decreased levels of PPAR γ in RPMs from young *Spic*-deficient mice, we speculated that *Spic*-deficient RPMs could be similar to the RPMs detected in *Vav1-Cre/Pparg*^{fl/fl} newborns. When we focused on similarities in the highly dysregulated genes ($|\log_2 \text{ratio}| > 2.5$; FDR < 0.05) from *Spic*^{-/-}, *Vav1-Cre/Pparg*^{fl/fl} RPMs and from adult tamoxifen-treated *CreERT2/Pparg*^{fl/fl} CD88^{hi} RPMs, the shared upregulated genes included *C5ar1*, *Itgal* (integrin α_L), and *Cx3cr1*, which are associated with the phenotype of patrolling monocytes (Fig. 6 A). Among the downregulated genes, 27 were shared between at least two sets (Fig. 6 B). The strongest gene reduction, common to all three cell subsets, was the gene encoding *Itgad* (integrin α_D). We examined CD88 and CD11a, encoded by the *Itgal* gene, protein expression on WT RPMs at different time points (Fig. 6 C) and observed that both markers were downregulated at days 5 and 7 after birth in WTs but not in either KO samples (Fig. 6 D). In addition, both *Spic*- and *Pparg*-deficient RPMs display increased CD11b and decreased VCAM-1 expression levels, when compared with WT controls derived from age-matched littermates (Fig. 6 E).

Taken together, the data demonstrate that *Spic* and *Pparg* repress expression of surface molecules (CD88) and orchestrate

adhesion and migration of the RPM precursor by regulation of the integrins CD11b, CD11a, and CD11d.

Discussion

Recent studies have identified signature transcription factors important for the differentiation of a variety of cell types and have elucidated the mechanism by which environmental signals trigger their expression (A-Gonzalez et al., 2013; Abutbul et al., 2012; Buttgeriet et al., 2016; Kierdorf et al., 2013; Okabe and Medzhitov, 2014; Schneider et al., 2014). To our knowledge, we are the first to describe the dependency of different tissue-resident macrophage subsets—iron-recycling macrophages and AMs—on the same transcription factor (PPAR γ), even though the macrophages have seemingly different functions.

AMs start to develop perinatally from yolk sac-derived fetal liver monocytes (Guilliams et al., 2013; Schneider et al., 2014). Sensing of GM-CSF produced mainly by alveolar epithelial cells induces PPAR γ activation and consequent transcriptional changes of target genes that orchestrate terminal differentiation and functional specialization. Deletion of *Pparg* at birth—induced by *Cd11c-Cre*—arrests AM development at the level of a dysfunctional pro-AM with defects in lipid metabolism (Schneider et al., 2014). The two other *Pparg*-dependent macrophage populations reported here, splenic RPMs and bone marrow EIMs, share an iron-recycling function. RPMs derive from fetal liver monocytes and are long lived (Epelman et al., 2014). Their development from monocytes has been shown previously to depend on another transcription factor, Spi-C (Kohyama et al., 2009). Spi-C is constitutively repressed in monocytes by Bach1, but is induced by increasing levels of heme, an intermediate product of hemoglobin degradation. Heme binds to Bach1 and marks the transcriptional repressor for proteasomal degradation (Haldar et al., 2014). Interestingly, we show that Spi-C is dispensable for the RPM and EIM expansion that occurs in the first week after birth. Nonetheless, *Spic*^{-/-} RPMs differ significantly from their WT counterparts at the transcriptomic level. The expression of genes related to iron metabolism, like heme oxygenase 1 (*Hmox1*), ferritin (*Fth1*, *Ftl1*), and ferroportin (*Slc40a1*), is decreased, indicating compromised functionality of *Spic*^{-/-} RPMs. Similarly, *Hmox1*^{-/-} mice lose iron-recycling macrophage populations with time, because they are unable to break down cytotoxic heme, leading to elevated oxidative stress and cell death (Kovtunovych et al., 2010). Interestingly, *Pparg*-deficient RPM-like cells from *Vav1-Cre/Pparg*^{fl/fl} mice are able to phagocytose RBCs but are impaired in support of normal iron recycling.

The lack of Spi-C or PPAR γ expression leads to a similar phenotype in adult mice. Both *Spic*^{-/-} and *Vav1-Cre/Pparg*^{fl/fl} mice have strongly reduced RPM and EIM populations and accumulate iron in the spleen and bone marrow (not shown),

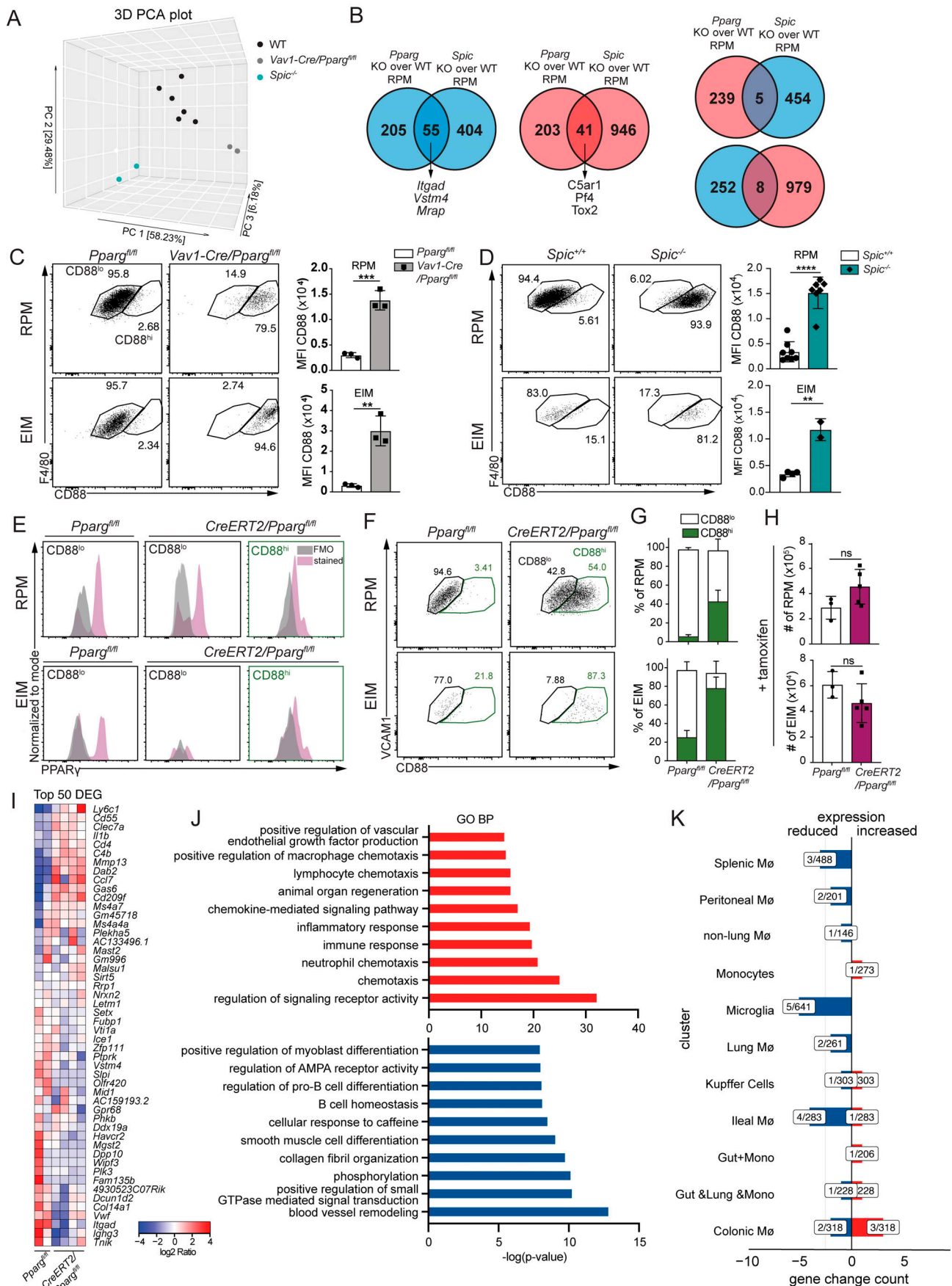


Figure 5. PPAR γ maintains RPM identity throughout life. **(A)** PCA performed on the transcriptome from two to three biological replicates from *Pparg*^{fl/fl} or *Spic*^{+/+} (WT; black dots), *Vav1-Cre/Pparg*^{fl/fl} (gray dots), and *Spic*^{-/-} RPMs (green dots). **(B)** Venn diagrams comparing upregulated (red) or downregulated (blue) genes in RPMs derived from *Vav1-Cre/Pparg*^{fl/fl} and *Spic*^{-/-} mice when compared with WT counterparts ($|\log_2 \text{ratio}| > 1.5$). The results are accompanied with a list of the top three commonly upregulated or downregulated genes. **(C and D)** Expression of CD88 on *Pparg*^{fl/fl} and *Vav1-Cre/Pparg*^{fl/fl} (C) and *Spic*^{+/+} and *Spic*^{-/-} (D) RPMs and EIMs detected by flow cytometry and plotted as MFI. **(E–K)** *Pparg*^{fl/fl} and *CreERT2/Pparg*^{fl/fl} mice (8 wk old) were treated with tamoxifen every other day for 2 wk and analyzed 4 d later. Flow cytometry data showing PPAR γ protein expression within CD88^{hi} and CD88^{lo} RPM and EIM populations (E), CD88 cell surface expression on F4/80⁺VCAM-1⁺ RPMs and EIMs (F), and frequencies of CD88^{hi} and CD88^{lo} cells among RPMs (G). **(H)** Total numbers of RPMs and EIMs. **(I–K)** CD88^{lo} RPMs from *Pparg*^{fl/fl} and CD88^{hi} RPMs from *CreERT2/Pparg*^{fl/fl} mice (all tamoxifen treated) were isolated and RNA sequencing was performed. **(I)** Heat map showing top DEGs between *Pparg*^{fl/fl} and *CreERT2/Pparg*^{fl/fl} RPMs (according to absolute values of *g*fold). **(J)** Upregulated (red) and downregulated (blue) GO terms for Biological Process (BP) from a comparison of CD88^{hi} RPMs from *CreERT2/Pparg*^{fl/fl} over CD88^{lo} RPMs from *Pparg*^{fl/fl} ($P < 0.01$). **(K)** Bar graphs showing upregulated (red) and downregulated (blue) genes from a comparison of CD88^{hi} RPMs from *CreERT2/Pparg*^{fl/fl} over CD88^{lo} RPMs from *Pparg*^{fl/fl} ($|\log_2 \text{ratio}| > 1.5$) with gene signatures of different tissue-resident macrophages (M Φ) and monocytes derived from Lavin et al. (2014). The presented data are from a single experiment (A, B, and I–K) or representative of two independent experiments (C–H; mean and SD from two to five mice per group). **, $P < 0.01$; ***, $P < 0.001$; ****, $P < 0.0001$ (unpaired two-tailed Student's *t* test).

while their blood contains normal levels of erythrocytes. Also, the decrease in RPMs does not influence the cellular composition of the spleen, indicating that deletion of PPAR γ in other CD45⁺ immune cells—that express *Vav1-cre*—did not change the cell composition and indirectly cause the loss of RPMs. To definitively exclude this possibility, we experimentally confirmed that PPAR γ is required intrinsically for RPM development.

Global PPAR γ deficiency in mice is embryonically lethal (Barak et al., 1999). Using the *Cre-loxP* system, PPAR γ deficiency has been studied in various cell subtypes and was identified as a master regulator of adipocyte differentiation (Siersbaek et al., 2010). Studies addressing the importance of PPAR γ in the immune system show that this nuclear receptor is essential for AM development upon GM-CSF activation (Schneider et al., 2014) and M2 macrophage polarization triggered by IL-4 stimulation (Odegaard et al., 2007; Szanto et al., 2010). PPAR γ is highly expressed in AMs and splenic macrophages, but it is low in most other hematopoietic cells in the steady state (Gautier et al., 2012a). We show that PPAR γ starts being expressed by RPMs during the first few days after birth and persists at high levels into adulthood. This increased expression within the first days of life correlates with an abrupt expansion of this subset and a marked defect in RPM numbers in the absence of PPAR γ . IL-4 and GM-CSF are well-established drivers of PPAR γ expression in M2 macrophages and AMs, respectively; however, both IL-4R⁻ and GM-CSFR⁻ deficient mice showed no reduction in the RPM and EIM population, demonstrating that these cytokines are dispensable for RPM and EIM development. Nonetheless, overexpression of IL-4 by hydrodynamic gene delivery led to an expansion of RPMs in WT mice. It remains to be investigated which factors activate PPAR γ in the RPM and EIM niches in the red pulp and bone marrow and whether or not activation requires a PPAR γ lipid ligand (Daniel et al., 2018).

Loss of PPAR γ expression led to changes in the transcriptome of sorted RPMs and EIMs. GO analysis for DEGs in RPM/EIM-like cells from *Vav1-Cre/Pparg*^{fl/fl} mice compared with WT counterparts revealed a more pro-inflammatory phenotype of *Pparg*-deficient RPM-like and EIM-like cells as early as 7 d after birth. Biological processes, like chemotaxis and cell migration, were increased, while DNA repair

and cell-cycle pathways were strongly reduced. The reduction in transcripts from genes involved in cell cycling was not reflected in a reduced Ki67 or 5-ethynyl-2'-deoxyuridine (EdU) incorporation in *Pparg*-deficient RPM-like cells from *Vav1-Cre/Pparg*^{fl/fl} newborn mice. This result needs further investigation but could be an indication of increased cell death or altered cell-cycle times in *Pparg*-deficient RPM-like cells. Recently, it was shown that large peritoneal macrophages lacking *Bhlhe40* are reduced in number due to a proliferative defect, despite normal BrdU incorporation. This was explained by the accumulation of cells in G1 phase and similar numbers in S, G2, and M phases (Jarjour et al., 2019).

The expression of multiple RPM signature genes was reduced upon PPAR γ deficiency, while expression of genes associated with signatures of other tissue-resident macrophage subsets was increased. Analysis of *CreERT2/Pparg*^{fl/fl} CD88^{hi} RPMs from tamoxifen-treated mice further confirmed the role of PPAR γ in maintaining RPM identity.

Interestingly, *Spic*-deficient and *Pparg*-deficient RPMs share many similarities, which may be explained by reduction of *Pparg*-levels in the absence of *Spi-C*. Both PPAR γ - and *Spi-C*-deficient RPM-like cells fail to downregulate CD11a and CD88 on both the transcriptional and protein levels. We identified another member of the integrin family, integrin α_D (CD11d, encoded by *Itgad*), as strongly downregulated in deficient RPMs. Importantly, integrin α_D expression is specific to RPMs and, according to the Immunological Genome Project (<http://www.immgen.org>), is not expressed in any other tissue-resident macrophage subset. Elevated levels of integrin α_D have been linked to increased cell adhesiveness and macrophage retention in vascular lesions (Aziz et al., 2017; Yakubenko et al., 2008). Interestingly, the *Itgad* promoter contains several predicted binding sites for PPAR γ and could be a novel target of this transcription factor. The interaction of integrin VLA4 ($\alpha_4\beta_1$) and VCAM-1 is important for erythroblastic island formation (Sadahira et al., 1995). Mice lacking VCAM-1 show a reduced number of RPMs and EIMs (Ulyanova et al., 2016). Thus, impaired expression of VCAM-1 during the first week after birth can explain the defect in expansion and migration RPMs and probably also EIMs in the absence of PPAR γ .

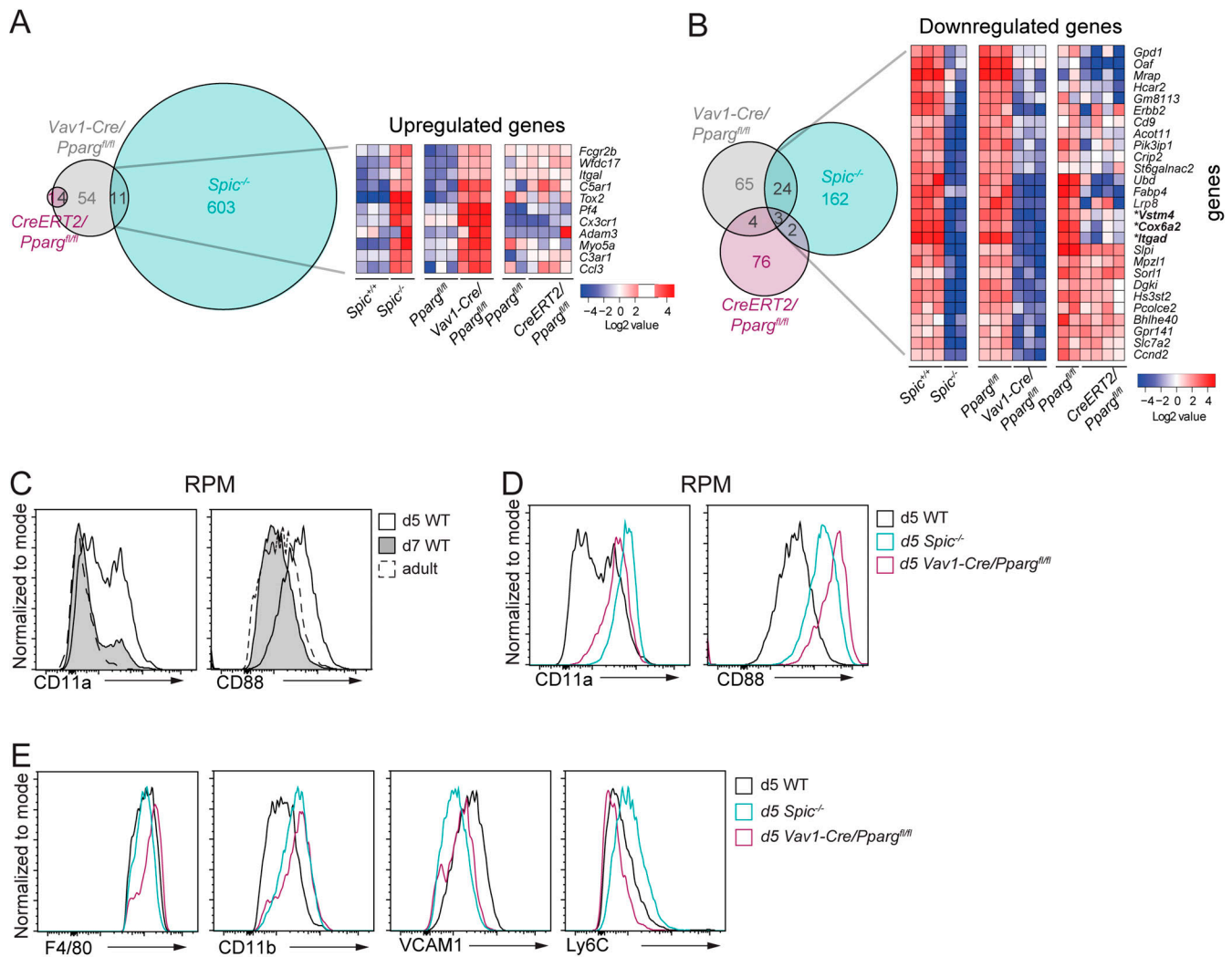


Figure 6. Transcriptional changes associated with *Pparg* and *Spic* deficiency in RPMs. (A and B) Venn diagrams comparing upregulated (A) or downregulated (B) genes in RPMs derived from *Vav1-Cre/Pparg^{fl/fl}*, *Spic^{-/-}*, and *CreERT2/Pparg^{fl/fl}* mice (after tamoxifen administration) when compared with WT counterparts (\log_2 ratio > 2.5 ; FDR < 0.05). The results are accompanied with heat maps presenting 11 upregulated (A) or 27 downregulated genes (B) shared by *Vav1-Cre/Pparg^{fl/fl}* and *Spic^{-/-}* RPMs with three gene names in bold (and starred) shared by all three deficient RPM populations. **(C and D)** Representative histograms of CD11a (*Itgal*; C) and CD88 (*C5ar1*; D) expression during WT RPM maturation. **(E)** Representative histograms of the expression of the indicated markers on RPMs from 5-d-old mice. The presented data are from a single experiment with three to five mice per group.

We propose that both Spi-C and PPAR γ are upregulated when RPM precursors enter the neonatal spleen and that PPAR γ expression is partially controlled by Spi-C. Together, they induce upregulation of VCAM-1 and changes in expression of the integrins CD11a (going down) and CD11d (going up), thereby facilitating the docking of progenitors in the niche and allowing further differentiation. Upon loss of either of the two factors, the potential progenitor cannot be efficiently retained in the tissue and possibly migrates out or dies due to displacement and/or lack of a niche factor. Neonatal expansion and the delayed death of *Spic*-deficient RPMs compared with *Pparg*-deficient RPMs may be explained by a compensatory mechanism activated in the absence of Spi-C.

Collectively, the presented data unequivocally demonstrate PPAR γ as a central regulator of iron-recycling macrophage development. The program triggered in the spleen and bone marrow seems to be very distinct from the program induced by the same

factor in AM differentiation and includes novel pathways not related to lipid metabolism, possibly due to the collaborative action of Spi-C and PPAR γ on tissue-specific target gene expression.

Materials and methods

Mice

Pparg^{tm1.2Mtz}(Pparg^{fl/fl}) mice (Imai et al., 2004), kindly provided by P. Chambon (University of Strasbourg, Strasbourg, France), were backcrossed for eight generations to C57BL/6 before crossing to either *Lyz2Cre^{tm1}(Cre)^{lfo}* (*LysM-Cre*) mice (Clausen et al., 1999), *Tg(Itgax-cre)1-IReiz* (*Cd11c-Cre*) mice (Caton et al., 2007), *B6.Cg-Tg(Vav1-Cre)A2Kio/J* (*Vav1-Cre*) mice (de Boer et al., 2003), or *B6.Cg-Ndor1^{Tg}(UBC-cre/ERT2)^{IEjb}/2J* (*CreERT2*) (Ruzankina et al., 2007), resulting in mice with PPAR γ deficiency either in myeloid cells (*LysM-Cre/Pparg^{fl/fl}*), CD11c⁺ cells

(*Cd11c-Cre/Pparg^{fl/fl}*), hematopoietic cells (*Vav1-Cre/Pparg^{fl/fl}*), or all cells upon tamoxifen treatment (*CreERT2/Pparg^{fl/fl}*). For deletion of the *Pparg* gene in *CreERT2/Pparg^{fl/fl}* mice, 8-wk-old mice were injected i.p. with 2 mg tamoxifen (Sigma-Aldrich) every other day six times and analyzed 4 d later. The large majority of experiments were performed with littermate *Pparg^{fl/fl}* and *Vav1-Cre/Pparg^{fl/fl}* or *CreERT2/Pparg^{fl/fl}* mice. *Gt(ROSA)26Sor^{tm1Hjf}* (*Rosa26-RFP*) mice, which contain Cre-inducible tandem dimer RFP (Luche et al., 2007), were crossed with *Vav1-Cre* in order to check the Cre recombinase activity. *Spic^{-/-}* mice (Kohyama et al., 2009) were backcrossed for four generations to C57BL/6 (except Fig. S1 D, six-generation backcross littermates). All mice were housed in individually ventilated cages under specific pathogen-free conditions at the Swiss Federal Institute of Technology Phenomics Center (Zurich, Switzerland) and were used for experiments between 8 and 17 wk of age, unless otherwise stated. Animal experiments were approved by the local animal ethics committee (Cantonal Veterinary Office, Zurich, Switzerland) and were performed according to local guidelines (Swiss Animal Protection Ordinance, Zurich, Switzerland) and Swiss animal protection law.

Cell suspensions

Mice were killed by CO₂ overdose. Organs were removed and cut into small pieces, and then digested and passed through a 70- μ m cell strainer. Spleens and fetal livers were digested for 30 min at 37°C with 2 mg/ml of type IV collagenase (Worthington Biochemical) and 50 U/ml DNase I (Sigma-Aldrich). Adult livers were digested for 45 min at 37°C with 2 mg/ml of type IV collagenase and 50 U/ml DNase I. Liver cell suspensions were centrifuged at 20 *g* for 5 min, and the supernatants with reduced number of hepatocytes were resuspended in 30% Percoll (GE Healthcare) before density centrifugation at 2,000 rpm for 20 min at 25°C, with low acceleration and no brake. Bone marrow was flushed from the femur and tibia of mice and passed through a 70- μ m cell strainer. Erythrocytes were lysed with ammonium chloride–potassium bicarbonate buffer.

Iron staining

Deposits of ferric iron were visualized by histochemistry using Prussian Blue stain of 4- μ m sections of formalin-fixed, paraffin-embedded tissues. Multiple images of each biological replicate were taken using a 20 \times objective (Zeiss Plan Neofluar 20 \times /0.50 Ph2) on a Zeiss microscope equipped with a charge-coupled device camera (QImaging RETIGA EXi). Image quantification was performed using Fiji/ImageJ. Briefly, images were color thresholded in Blue to select blue pixels. Particle Analyzer (v1.50e) was used to quantify the area and the integrated intensity of the segmented pixels in Red, Green, and Blue channels. The same measurements were taken on areas outside of the segmented pixels to provide the background intensity profiles. Rug plots were generated using the *Seaborn.distplot* function in Python.

Immunohistochemistry

Isolated spleens were fixed overnight in freshly prepared 4% paraformaldehyde (Merck Millipore) at 4°C under constant agitation. Fixed spleens were embedded in 4% agarose and cut with

a vibratome (Leica VT-1200). 40- μ m sections were blocked with PBS supplemented with 10% FCS, 1 mg/ml anti-Fc γ R (BD Biosciences), and 0.1% Triton X-100 (Sigma-Aldrich) for 30 min at room temperature. Next, a primary antibody mix containing anti-B220, anti-F4/80, and anti-metallophilic macrophage marker (CD169) was added and samples were incubated in 4°C overnight. After washing with PBS supplemented with 2% FCS and 0.1% Triton X-100, secondary antibodies were applied for 1 h at room temperature. Stained sections were transferred onto slides and coverslips were mounted with Dako fluorescent mounting media. Microscopic analysis was performed using a confocal microscope (Zeiss LSM 710), and images were processed with ZEN 2010 software (Carl Zeiss).

Cell proliferation in vivo

Pups were injected with EdU and splenocytes were analyzed 14 h later using Click-iT Plus EdU Alexa Fluor 488 Flow Cytometry Assay Kit (Thermo Fischer Scientific) according to the manufacturer's instructions.

Flow cytometry

Multiparameter analysis was performed with LSR Fortessa (BD Biosciences), followed by data analysis with FlowJo software (TreeStar). All fluorochrome-conjugated or biotinylated monoclonal antibodies used are listed in Table 1. Dead cells were gated out using the viability marker eFluor780 (eBioscience). Fc γ III/II receptors were blocked by incubation with anti-CD16/32 (2.4G2) purified from hybridoma supernatant (Swiss Federal Institute of Technology) before staining. PPAR γ intracellular staining was performed using the Foxp3/Transcription Factor Staining Buffer Set (Thermo Fisher Scientific) according to the manufacturer's protocol.

Cell sorting

Fetal liver cells were enriched for CD45⁺ cells using magnetic cell sorting (MACS) LS columns and anti-CD45 beads (both Miltenyi Biotec). Briefly, single-cell suspensions were incubated with 10 μ l of beads/10⁷ cells for 15 min at 4°C, followed by a wash with MACS buffer (PBS containing 1% BSA and 2 mM EDTA; both from Sigma-Aldrich). Pelleted cells were resuspended in 500 μ l MACS buffer and loaded on equilibrated LS columns. Samples were washed twice with gravity flow of 4 ml MACS buffer and, after removing columns from the magnetic field, the purified fraction was eluted. CD45⁺ cells were later used for injections in *Vav1-Cre/Pparg^{fl/fl}* newborns in 10 μ l PBS (0.6 \times 10⁶/newborn). Fluorescence-activated cell sorting of RPMs/EIMs for cytopins, RBC phagocytosis, and RNA sequencing analysis was performed with a FACSAria IIIu (BD Biosciences).

RBC phagocytosis assay

In vivo

RBCs from whole blood were prepared as previously described (Theurl et al., 2016). In short, cells were washed with three volumes of PBS three times and centrifuged at 400 *g* for 10 min and subsequently stressed by incubation at 48°C for 20 min under continuous shaking. Next, stressed RBCs were resuspended in 1 ml of Diluent C (Sigma-Aldrich) and incubated

Table 1. Antibodies used in this study

Channel	Name	Dilution	Company	Clone
AF488	F4/80	300	BioLegend	BM8
FITC	VCAM-1	200	eBioscience	429
PE	CD88	200	BioLegend	20/70
PE-Cy7	CD11c	1,000	BioLegend	117318
PerCP-Cy5.5	CD11b	1,000	BioLegend	M1/70
APC	CD45.1	200	BioLegend	A20
APC	goat rabbit IgG(H+L)-Alexa 647	1,000	Thermo Fisher Scientific	Polyclonal
BV421	CD64	200	BioLegend	X54-5/7.1
BV421	F4/80	300	BioLegend	BM8
BV510	MHCII	400	BioLegend	M5/114.15.2
BV605	CD11c	500	BioLegend	N418
BV785	CD45.2	100	BioLegend	104
BV785	CD45	1,000	Biologend	30-F11
BV711	Streptavidin	1,000	BD Biosciences	
Biotinylated	Ly6C	2,000	BioLegend	HK1.4
Biotinylated	CD11a	1,000	BioLegend	M17/4
Unlabeled	PPAR γ	25	Cell Signaling Technology	81B8

for 5 min at room temperature with an equal volume of 4 μ M PKH26 (Sigma-Aldrich) in the dark. Unbound particles were quenched with 2 ml of 100% FCS and the sample was spun down (400 *g*, 10 min) and washed two times with quenching buffer (PBS with 10% FCS). Finally, RBCs were resuspended in PBS and $\sim 0.8 \times 10^9$ RBCs were injected into the tail vein of *Vav1-Cre/Pparg^{fl/fl}* and control mice. Some of the mice were sacrificed 16 h after injection and spleens and livers were isolated for single-cell suspension preparation. Blood samples were taken at 20 min, 16 h, 64 h, 88 h, and 90 h after injection.

In vitro

Sorted RPMs were plated on round glass coverslips in a 24-well plate containing RPMI 1640 plus GlutaMAX, 10% FCS, 100 U/ml penicillin, 100 μ g/ml streptomycin, and 50 μ M β -mercaptoethanol (all Gibco) and left overnight to attach. The next day, RBCs were isolated from 200 μ l of whole blood by several centrifugations with isotonic buffer (0.9% NaCl, 5 mM Na₃PO₄, pH 8) at low speed (600 *g*, 10 min). Cells were then lysed with 1 ml of hypotonic buffer (5 mM Na₃PO₄, pH 8) and spun down for 10 min at 12,000 *g*. Lysis and centrifugation were repeated until the pellet was white. Ghost RBCs were resuspended in 500 μ l PBS + 0.1% BSA and incubated for 10 min at 37°C with an equal volume of 10 μ M CFSE (Life Technologies). Unbound particles were quenched with 1 ml PBS with 10% FCS and the sample was spun down (12,000 *g*, 10 min) and washed two times with quenching buffer. Finally, RBCs were resuspended in the same medium as RPMs and incubated with cultured cells for 1 h at 37°C. Afterwards, cells were washed twice with PBS to remove unbound RBCs and fixed with 4% paraformaldehyde (Sigma-Aldrich) for 15 min at room temperature. Glass coverslips were then washed with PBS and cells

were perforated with PBS containing 10% FCS and 0.1% Triton X-100 for 1 h at room temperature. Next, cells were stained with FluorProbes 647-conjugated phalloidin (Interchim) for 1 h at room temperature. After extensive washing with PBS, cells were stained with DAPI (Sigma-Aldrich) and mounted on slides with Dako fluorescent mounting media. Samples were analyzed with Zen 2 software (Zeiss) on a fluorescence microscope (Zeiss AxioImager M2).

Quantitative real-time PCR

RNA was isolated with TRIzol reagent (Invitrogen) and reverse transcribed with GoScript RT (Promega) according to the manufacturer's instructions. The resulting cDNA was used for quantitative real-time PCR with KAPA SYBR FAST (Sigma-Aldrich) performed on an i-Cycler (Bio-Rad). Expression was normalized to the housekeeping gene *G6PDX* expression, and the values were calculated using the comparative threshold cycle method ($2^{-\Delta C_t}$). Primer sequences: *G6PDX* forward primer: 5'-CTACAGGTTTCAGATGATGTC-3', reverse primer: 5'-CAGCTTCTCCTTCTCCATTG-3'; and *Pparg* forward primer: 5'-GTGATGGAAGACCACTCGCATT-3', reverse primer: 5'-CCATGAGGGAGTTAGAAGTTTC-3'.

RNA preparation and sequencing

1,000 cells (RPMs/EIMs) were sorted directly into the lysis buffer (0.2% Triton X-100, 2 U/ μ l RNase inhibitor [New England Biolabs] in RNase-free water [Thermo Fisher Scientific]). RNA isolation and sequencing were performed as described before (Picelli et al., 2014). Briefly, oligo-dT primers and dNTPs were added to lysed cells and hybridization of the primer to poly(A) tails of all mRNA was performed at 72°C for 3 min. Next, samples were reverse transcribed with LNA-containing TSO primer,

enabling template switching, and SuperScript II RT (Thermo Fisher Scientific) at 42°C for 90 min followed by 10 cycles of 2-min intervals at 50°C and 42°C in order to increase efficiency and complete the reaction. cDNA was preamplified using ISPCR primers containing the matching sequence to the outer fragments of oligo-dT and TSO primers. Amplification was performed with 18 cycles of 20 s denaturation at 98°C, 15 s annealing at 67°C, and 6 min extension at 72°C with KAPA HiFi HotStart ReadyMix (Kapa Biosystems). PCR products were purified with AMPure XP beads (Beckman Coulter), and 1 ng of the product was tagged using the Nextera XT DNA sample preparation kit (Illumina). Afterward, final enrichment with Index primers from the Nextera XT kit (Illumina) was performed for eight cycles of 30 s denaturation at 95°C, 30 s annealing at 55°C, and 30 s extension at 72°C, followed by purification with AMPure XP beads. Two nanomoles of each library were pooled for single-end DNA sequencing on a HiSeq4000 or NovaSeq instrument. Sequencing was performed at the Functional Genomics Center Zurich. The sequences were analyzed with the SUSHI application (Hatakeyama et al., 2016). In short, fragments were mapped to the Ensemble mouse reference genome GRCm38 (v25.06.2015) with the STAR aligner (Dobin et al., 2013). Values were then computed with the featureCounts function (Rsubread; Liao et al., 2013), and DEGs were detected with the Bioconductor package edgeR (Robinson et al., 2010). All heat maps present the top 50 genes according to the absolute value of the generalized fold change (gfold; Feng et al., 2012). Sequences were deposited to the Gene Expression Omnibus (accession no. GSE166085).

Statistical analysis

All statistical analyses were performed with Prism software (GraphPad). Comparisons of two groups were calculated with unpaired two-tailed Student's *t* tests. Differences with a *P* value of <0.05 were considered significant.

Online supplemental material

Fig. S1 depicts the gating strategy for identification of RPMs and numbers of RPMs and EIMs in *Spic*^{-/-} and WT mice at different ages. **Fig. S2** shows RPM and EIM numbers in *Cd11c-Cre/Pparg*^{fl/fl} and *LysM-Cre/Pparg*^{fl/fl} mice, as well as Cre activity in RPMs from *Vav1-Cre/Rosa26-RFP* mice. **Fig. S3** shows RPM frequencies and numbers of lymphocytes and myeloid subsets in the spleen of *Vav1-Cre/Pparg*^{fl/fl} mice. **Fig. S4** shows differential gene expression in *Pparg*-deficient EIMs; phagocytosis of RBCs; and stress erythropoiesis in *Vav1-Cre/Pparg*^{fl/fl} mice. **Fig. S5** shows spleen and bone marrow cellularity after conditional depletion of *Pparg* in adults.

Acknowledgments

We thank C. Riether (University of Bern, Bern, Switzerland) for *Spic*^{-/-} mice and M. Kieselow and A. Schütz (Swiss Federal Institute of Technology Flow Cytometry Core Facility, Zurich, Switzerland) for cell sorting.

This work was mainly funded by Swiss National Science Foundation grants 310030_163443 and 310030B_182829 (M.

Kopf) and P4P4PM_180832 (C. Schneider), as well as by the Peter Hans Hofschneider Professorship (C. Schneider).

Author contributions: K. Okreglicka, I. Iten, and M. Kopf designed the experiments; K. Okreglicka and I. Iten performed and analyzed most of the experiments; L. Pohlmeier, Q. Feng, M. Kurrer, L. Onder and C. Schneider performed and analyzed specific experiments; B. Ludewig and C. Schneider edited the manuscript and curated data; K. Okreglicka, P. Nielsen, and M. Kopf wrote the manuscript; M. Kopf acquired funding and conceptualized the study.

Disclosures: B. Ludewig reported grants from Swiss National Science Foundation, grants from Swiss Cancer League, and other from Stromal Therapeutics AG outside the submitted work. No other disclosures were reported.

Submitted: 17 July 2019

Revised: 9 December 2020

Accepted: 22 February 2021

References

- A-Gonzalez, N., J.A. Guillen, G. Gallardo, M. Diaz, J.V. de la Rosa, I.H. Hernandez, M. Casanova-Acebes, F. Lopez, C. Tabraue, S. Beceiro, et al. 2013. The nuclear receptor LXR α controls the functional specialization of splenic macrophages. *Nat. Immunol.* 14:831-839. <https://doi.org/10.1038/ni.2622>
- Abutbul, S., J. Shapiro, I. Szaingurten-Solodkin, N. Levy, Y. Carmy, R. Baron, S. Jung, and A. Monsonego. 2012. TGF- β signaling through SMAD2/3 induces the quiescent microglial phenotype within the CNS environment. *Glia.* 60:1160-1171. <https://doi.org/10.1002/glia.22343>
- Amit, I., D.R. Winter, and S. Jung. 2016. The role of the local environment and epigenetics in shaping macrophage identity and their effect on tissue homeostasis. *Nat. Immunol.* 17:18-25. <https://doi.org/10.1038/ni.3325>
- Aziz, M.H., K. Cui, M. Das, K.E. Brown, C.L. Ardell, M. Febbraio, E. Pluskota, J. Han, H. Wu, C.M. Ballantyne, et al. 2017. The Upregulation of Integrin $\alpha\beta_2$ (CD11d/CD18) on Inflammatory Macrophages Promotes Macrophage Retention in Vascular Lesions and Development of Atherosclerosis. *J. Immunol.* 198:4855-4867. <https://doi.org/10.4049/jimmunol.1602175>
- Barak, Y., M.C. Nelson, E.S. Ong, Y.Z. Jones, P. Ruiz-Lozano, K.R. Chien, A. Koder, and R.M. Evans. 1999. PPAR γ is required for placental, cardiac, and adipose tissue development. *Mol. Cell.* 4:585-595. [https://doi.org/10.1016/S1097-2765\(00\)80209-9](https://doi.org/10.1016/S1097-2765(00)80209-9)
- Bessis, M. 1958. Erythroblastic island, functional unity of bone marrow. *Rev. Hematol. (Paris).* 13:8-11.
- Bonfield, T.L., C.F. Farver, B.P. Barna, A. Malur, S. Abraham, B. Raychaudhuri, M.S. Kavuru, and M.J. Thomassen. 2003. Peroxisome proliferator-activated receptor-gamma is deficient in alveolar macrophages from patients with alveolar proteinosis. *Am. J. Respir. Cell Mol. Biol.* 29:677-682. <https://doi.org/10.1165/rcmb.2003-0148OC>
- Butovsky, O., M.P. Jedrychowski, C.S. Moore, R. Cialic, A.J. Lanser, G. Gabriely, T. Koeglsperger, B. Dake, P.M. Wu, C.E. Doykan, et al. 2014. Identification of a unique TGF- β -dependent molecular and functional signature in microglia. *Nat. Neurosci.* 17:131-143. <https://doi.org/10.1038/nn.3599>
- Buttgereit, A., I. Lelios, X. Yu, M. Vrohligs, N.R. Krakoski, E.L. Gautier, R. Nishinakamura, B. Becher, and M. Greter. 2016. Sall1 is a transcriptional regulator defining microglia identity and function. *Nat. Immunol.* 17:1397-1406. <https://doi.org/10.1038/ni.3585>
- Caton, M.L., M.R. Smith-Raska, and B. Reizis. 2007. Notch-RBP-J signaling controls the homeostasis of CD8- dendritic cells in the spleen. *J. Exp. Med.* 204:1653-1664. <https://doi.org/10.1084/jem.20062648>
- Chow, A., D. Lucas, A. Hidalgo, S. Méndez-Ferrer, D. Hashimoto, C. Scheiermann, M. Battista, M. Leboeuf, C. Prophete, N. van Rooijen, et al. 2011. Bone marrow CD169+ macrophages promote the retention of hematopoietic stem and progenitor cells in the mesenchymal stem cell niche. *J. Exp. Med.* 208:261-271. <https://doi.org/10.1084/jem.20101688>

- Chow, A., M. Huggins, J. Ahmed, D. Hashimoto, D. Lucas, Y. Kunisaki, S. Pinho, M. Leboeuf, C. Noizat, N. van Rooijen, et al. 2013. CD169⁺ macrophages provide a niche promoting erythropoiesis under homeostasis and stress. *Nat. Med.* 19:429–436. <https://doi.org/10.1038/nm.3057>
- Clausen, B.E., C. Burkhardt, W. Reith, R. Renkawitz, and I. Förster. 1999. Conditional gene targeting in macrophages and granulocytes using LysMcre mice. *Transgenic Res.* 8:265–277. <https://doi.org/10.1023/A:1008942828960>
- Daniel, B., G. Nagy, Z. Czimmerer, A. Horvath, D.W. Hammers, I. Cuaranta-Monroy, S. Poliska, P. Tzerpos, Z. Kolostyak, T.T. Hays, et al. 2018. The Nuclear Receptor PPAR γ Controls Progressive Macrophage Polarization as a Ligand-Insensitive Epigenomic Ratchet of Transcriptional Memory. *Immunity.* 49:615–626.e6. <https://doi.org/10.1016/j.immuni.2018.09.005>
- de Boer, J., A. Williams, G. Skavdis, N. Harker, M. Coles, M. Tolaini, T. Norton, K. Williams, K. Roderick, A.J. Potocnik, and D. Kioussis. 2003. Transgenic mice with hematopoietic and lymphoid specific expression of Cre. *Eur. J. Immunol.* 33:314–325. <https://doi.org/10.1002/immu.200310005>
- Dobin, A., C.A. Davis, F. Schlesinger, J. Drenkow, C. Zaleski, S. Jha, P. Batut, M. Chaisson, and T.R. Gingeras. 2013. STAR: ultrafast universal RNA-seq aligner. *Bioinformatics.* 29:15–21. <https://doi.org/10.1093/bioinformatics/bts635>
- Epelman, S., K.J. Lavine, A.E. Beaudin, D.K. Sojka, J.A. Carrero, B. Calderon, T. Brija, E.L. Gautier, S. Ivanov, A.T. Satpathy, et al. 2014. Embryonic and adult-derived resident cardiac macrophages are maintained through distinct mechanisms at steady state and during inflammation. *Immunity.* 40:91–104. <https://doi.org/10.1016/j.immuni.2013.11.019>
- Feng, J., C.A. Meyer, Q. Wang, J.S. Liu, X. Shirley Liu, and Y. Zhang. 2012. GFOLD: a generalized fold change for ranking differentially expressed genes from RNA-seq data. *Bioinformatics.* 28:2782–2788. <https://doi.org/10.1093/bioinformatics/bts515>
- Gautier, E.L., A. Chow, R. Spanbroek, G. Marcelin, M. Greter, C. Jakubzick, M. Bogunovic, M. Leboeuf, N. van Rooijen, A.J. Habenicht, et al. 2012a. Systemic analysis of PPAR γ in mouse macrophage populations reveals marked diversity in expression with critical roles in resolution of inflammation and airway immunity. *J. Immunol.* 189:2614–2624. <https://doi.org/10.4049/jimmunol.1200495>
- Gautier, E.L., T. Shay, J. Miller, M. Greter, C. Jakubzick, S. Ivanov, J. Helft, A. Chow, K.G. Elpek, S. Gordonov, et al. Immunological Genome Consortium. 2012b. Gene-expression profiles and transcriptional regulatory pathways that underlie the identity and diversity of mouse tissue macrophages. *Nat. Immunol.* 13:1118–1128. <https://doi.org/10.1038/ni.2419>
- Ginhoux, F., and M. Guillems. 2016. Tissue-Resident Macrophage Ontogeny and Homeostasis. *Immunity.* 44:439–449. <https://doi.org/10.1016/j.immuni.2016.02.024>
- Ginhoux, F., M. Greter, M. Leboeuf, S. Nandi, P. See, S. Gokhan, M.F. Mehler, S.J. Conway, L.G. Ng, E.R. Stanley, et al. 2010. Fate mapping analysis reveals that adult microglia derive from primitive macrophages. *Science.* 330:841–845. <https://doi.org/10.1126/science.1194637>
- Glass, C.K., and G. Natoli. 2016. Molecular control of activation and priming in macrophages. *Nat. Immunol.* 17:26–33. <https://doi.org/10.1038/ni.3306>
- Gomez Perdiguero, E., K. Klapproth, C. Schulz, K. Busch, E. Azzoni, L. Crozet, H. Garner, C. Trouillet, M.F. de Bruijn, F. Geissmann, and H.R. Rodewald. 2015. Tissue-resident macrophages originate from yolk-sac-derived erythro-myeloid progenitors. *Nature.* 518:547–551. <https://doi.org/10.1038/nature13989>
- Gordon, S. 2007. The macrophage: past, present and future. *Eur. J. Immunol.* 37:S9–S17. <https://doi.org/10.1002/eji.200737638>
- Gosselin, D., V.M. Link, C.E. Romanoski, G.J. Fonseca, D.Z. Eichenfield, N.J. Spann, J.D. Stender, H.B. Chun, H. Garner, F. Geissmann, and C.K. Glass. 2014. Environment drives selection and function of enhancers controlling tissue-specific macrophage identities. *Cell.* 159:1327–1340. <https://doi.org/10.1016/j.cell.2014.11.023>
- Guillems, M., I. De Kleer, S. Henri, S. Post, L. Vanhoutte, S. De Prijck, K. Deswarte, B. Malissen, H. Hammal, and B.N. Lambrecht. 2013. Alveolar macrophages develop from fetal monocytes that differentiate into long-lived cells in the first week of life via GM-CSF. *J. Exp. Med.* 210:1977–1992. <https://doi.org/10.1084/jem.20131199>
- Haldar, M., M. Kohyama, A.Y. So, W. Kc, X. Wu, C.G. Briseño, A.T. Satpathy, N.M. Kretzer, H. Arase, N.S. Rajasekaran, et al. 2014. Heme-mediated SPI-C induction promotes monocyte differentiation into iron-recycling macrophages. *Cell.* 156:1223–1234. <https://doi.org/10.1016/j.cell.2014.01.069>
- Hashimoto, D., A. Chow, C. Noizat, P. Teo, M.B. Beasley, M. Leboeuf, C.D. Becker, P. See, J. Price, D. Lucas, et al. 2013. Tissue-resident macrophages self-maintain locally throughout adult life with minimal contribution from circulating monocytes. *Immunity.* 38:792–804. <https://doi.org/10.1016/j.immuni.2013.04.004>
- Hatakeyama, M., L. Opitz, G. Russo, W. Qi, R. Schlapbach, and H. Rehrauer. 2016. SUSHI: an exquisite recipe for fully documented, reproducible and reusable NGS data analysis. *BMC Bioinformatics.* 17:228. <https://doi.org/10.1186/s12859-016-1104-8>
- Hoeffel, G., J. Chen, Y. Lavin, D. Low, F.F. Almeida, P. See, A.E. Beaudin, J. Lum, I. Low, E.C. Forsberg, et al. 2015. MacMyb(+) erythro-myeloid progenitor-derived fetal monocytes give rise to adult tissue-resident macrophages. *Immunity.* 42:665–678. <https://doi.org/10.1016/j.immuni.2015.03.011>
- Hume, D.A., and S. Gordon. 1983. Mononuclear phagocyte system of the mouse defined by immunohistochemical localization of antigen F4/80. Identification of resident macrophages in renal medullary and cortical interstitium and the juxtaglomerular complex. *J. Exp. Med.* 157:1704–1709. <https://doi.org/10.1084/jem.157.5.1704>
- Hume, D.A., A.P. Robinson, G.G. MacPherson, and S. Gordon. 1983. The mononuclear phagocyte system of the mouse defined by immunohistochemical localization of antigen F4/80. Relationship between macrophages, Langerhans cells, reticular cells, and dendritic cells in lymphoid and hematopoietic organs. *J. Exp. Med.* 158:1522–1536. <https://doi.org/10.1084/jem.158.5.1522>
- Imai, T., R. Takakuwa, S. Marchand, E. Dentz, J.M. Bornert, N. Messaddeq, O. Wendling, M. Mark, B. Desvergne, W. Wahli, et al. 2004. Peroxisome proliferator-activated receptor γ is required in mature white and brown adipocytes for their survival in the mouse. *Proc. Natl. Acad. Sci. USA.* 101:4543–4547. <https://doi.org/10.1073/pnas.0400356101>
- Jakubzick, C., E.L. Gautier, S.L. Gibbings, D.K. Sojka, A. Schlitzer, T.E. Johnson, S. Ivanov, Q. Duan, S. Bala, T. Condon, et al. 2013. Minimal differentiation of classical monocytes as they survey steady-state tissues and transport antigen to lymph nodes. *Immunity.* 39:599–610. <https://doi.org/10.1016/j.immuni.2013.08.007>
- Jarjour, N.N., E.A. Schwarzkopf, T.R. Bradstreet, I. Shchukina, C.C. Lin, S.C. Huang, C.W. Lai, M.E. Cook, R. Taneja, T.S. Stappenbeck, et al. 2019. Bhlhe40 mediates tissue-specific control of macrophage proliferation in homeostasis and type 2 immunity. *Nat. Immunol.* 20:687–700. <https://doi.org/10.1038/s41590-019-0382-5>
- Kierdorf, K., D. Erny, T. Goldmann, V. Sander, C. Schulz, E.G. Perdiguero, P. Wieghofer, A. Heinrich, P. Riemke, C. Hölscher, et al. 2013. Microglia emerge from erythromyeloid precursors via Pu.1- and Irf8-dependent pathways. *Nat. Neurosci.* 16:273–280. <https://doi.org/10.1038/nn.3318>
- Kohyama, M., W. Ise, B.T. Edelson, P.R. Wilker, K. Hildner, C. Mejia, W.A. Frazier, T.L. Murphy, and K.M. Murphy. 2009. Role for Spi-C in the development of red pulp macrophages and splenic iron homeostasis. *Nature.* 457:318–321. <https://doi.org/10.1038/nature07472>
- Kovtunovych, G., M.A. Eckhaus, M.C. Ghosh, H. Ollivierre-Wilson, and T.A. Rouault. 2010. Dysfunction of the heme recycling system in heme oxygenase 1-deficient mice: effects on macrophage viability and tissue iron distribution. *Blood.* 116:6054–6062. <https://doi.org/10.1182/blood-2010-03-272138>
- Kurotaki, D., S. Kon, K. Bae, K. Ito, Y. Matsui, Y. Nakayama, M. Kanayama, C. Kimura, Y. Narita, T. Nishimura, et al. 2011. CSF-1-dependent red pulp macrophages regulate CD4 T cell responses. *J. Immunol.* 186:2229–2237. <https://doi.org/10.4049/jimmunol.1001345>
- Kurotaki, D., T. Uede, and T. Tamura. 2015. Functions and development of red pulp macrophages. *Microbiol. Immunol.* 59:55–62. <https://doi.org/10.1111/1348-0421.12228>
- Lavin, Y., D. Winter, R. Blecher-Gonen, E. David, H. Keren-Shaul, M. Merad, S. Jung, and I. Amit. 2014. Tissue-resident macrophage enhancer landscapes are shaped by the local microenvironment. *Cell.* 159:1312–1326. <https://doi.org/10.1016/j.cell.2014.11.018>
- Lavin, Y., A. Mortha, A. Rahman, and M. Merad. 2015. Regulation of macrophage development and function in peripheral tissues. *Nat. Rev. Immunol.* 15:731–744. <https://doi.org/10.1038/nri3920>
- Lee, S.H., P.M. Starkey, and S. Gordon. 1985. Quantitative analysis of total macrophage content in adult mouse tissues. Immunochemical studies with monoclonal antibody F4/80. *J. Exp. Med.* 161:475–489. <https://doi.org/10.1084/jem.161.3.475>
- Liao, Y., G.K. Smyth, and W. Shi. 2013. The Subread aligner: fast, accurate and scalable read mapping by seed-and-vote. *Nucleic Acids Res.* 41:e108. <https://doi.org/10.1093/nar/gkt214>
- Luche, H., O. Weber, T. Nageswara Rao, C. Blum, and H.J. Fehling. 2007. Faithful activation of an extra-bright red fluorescent protein in “knock-in” Cre-reporter mice ideally suited for lineage tracing studies. *Eur. J. Immunol.* 37:43–53. <https://doi.org/10.1002/eji.200636745>

- Murray, P.J., and T.A. Wynn. 2011. Protective and pathogenic functions of macrophage subsets. *Nat. Rev. Immunol.* 11:723–737. <https://doi.org/10.1038/nri3073>
- Odegaard, J.I., R.R. Ricardo-Gonzalez, M.H. Goforth, C.R. Morel, V. Subramanian, L. Mukundan, A. Red Eagle, D. Vats, F. Brombacher, A.W. Ferrante, and A. Chawla. 2007. Macrophage-specific PPARgamma controls alternative activation and improves insulin resistance. *Nature.* 447:1116–1120. <https://doi.org/10.1038/nature05894>
- Okabe, Y., and R. Medzhitov. 2014. Tissue-specific signals control reversible program of localization and functional polarization of macrophages. *Cell.* 157:832–844. <https://doi.org/10.1016/j.cell.2014.04.016>
- Parkhurst, C.N., G. Yang, I. Ninan, J.N. Savas, J.R. Yates III, J.J. Lafaille, B.L. Hempstead, D.R. Littman, and W.B. Gan. 2013. Microglia promote learning-dependent synapse formation through brain-derived neurotrophic factor. *Cell.* 155:1596–1609. <https://doi.org/10.1016/j.cell.2013.11.030>
- Picelli, S., O.R. Faridani, A.K. Björklund, G. Winberg, S. Sagasser, and R. Sandberg. 2014. Full-length RNA-seq from single cells using Smart-seq2. *Nat. Protoc.* 9:171–181. <https://doi.org/10.1038/nprot.2014.006>
- Robinson, M.D., D.J. McCarthy, and G.K. Smyth. 2010. edgeR: a Bioconductor package for differential expression analysis of digital gene expression data. *Bioinformatics.* 26:139–140. <https://doi.org/10.1093/bioinformatics/btp616>
- Ruzankina, Y., C. Pinzon-Guzman, A. Asare, T. Ong, L. Pontano, G. Cotsarelis, V.P. Zediak, M. Velez, A. Bhandoola, and E.J. Brown. 2007. Deletion of the developmentally essential gene ATR in adult mice leads to age-related phenotypes and stem cell loss. *Cell Stem Cell.* 1:113–126. <https://doi.org/10.1016/j.stem.2007.03.002>
- Sadahira, Y., T. Yoshino, and Y. Monobe. 1995. Very late activation antigen 4-vascular cell adhesion molecule 1 interaction is involved in the formation of erythroblastic islands. *J. Exp. Med.* 181:411–415. <https://doi.org/10.1084/jem.181.1.411>
- Schneider, C., S.P. Nobs, M. Kurrer, H. Rehrauer, C. Thiele, and M. Kopf. 2014. Induction of the nuclear receptor PPAR- γ by the cytokine GM-CSF is critical for the differentiation of fetal monocytes into alveolar macrophages. *Nat. Immunol.* 15:1026–1037. <https://doi.org/10.1038/ni.3005>
- Schulz, C., E. Gomez Perdiguero, L. Chorro, H. Szabo-Rogers, N. Cagnard, K. Kierdorf, M. Prinz, B. Wu, S.E. Jacobsen, J.W. Pollard, et al. 2012. A lineage of myeloid cells independent of Myb and hematopoietic stem cells. *Science.* 336:86–90. <https://doi.org/10.1126/science.1219179>
- Siersbaek, R., R. Nielsen, and S. Mandrup. 2010. PPARgamma in adipocyte differentiation and metabolism—novel insights from genome-wide studies. *FEBS Lett.* 584:3242–3249. <https://doi.org/10.1016/j.febslet.2010.06.010>
- Szanto, A., B.L. Balint, Z.S. Nagy, E. Barta, B. Dezso, A. Pap, L. Szeles, S. Poliska, M. Oros, R.M. Evans, et al. 2010. STAT6 transcription factor is a facilitator of the nuclear receptor PPAR γ -regulated gene expression in macrophages and dendritic cells. *Immunity.* 33:699–712. <https://doi.org/10.1016/j.immuni.2010.11.009>
- Takayanagi, H., S. Kim, T. Koga, H. Nishina, M. Isshiki, H. Yoshida, A. Saiura, M. Isobe, T. Yokochi, J. Inoue, et al. 2002. Induction and activation of the transcription factor NFATc1 (NFAT2) integrate RANKL signaling in terminal differentiation of osteoclasts. *Dev. Cell.* 3:889–901. [https://doi.org/10.1016/S1534-5807\(02\)00369-6](https://doi.org/10.1016/S1534-5807(02)00369-6)
- Theurl, I., I. Hilgendorf, M. Nairz, P. Tymoszyk, D. Haschka, M. Asshoff, S. He, L.M. Gerhardt, T.A. Holderried, M. Seifert, et al. 2016. On-demand erythrocyte disposal and iron recycling requires transient macrophages in the liver. *Nat. Med.* 22:945–951. <https://doi.org/10.1038/nm.4146>
- Ulyanova, T., S.R. Phelps, and T. Papayannopoulou. 2016. The macrophage contribution to stress erythropoiesis: when less is enough. *Blood.* 128:1756–1765. <https://doi.org/10.1182/blood-2016-05-714527>
- Yakubenko, V.P., N. Belevych, D. Mishchuk, A. Schurin, S.C. Lam, and T.P. Ugarova. 2008. The role of integrin alpha D beta2 (CD11d/CD18) in monocyte/macrophage migration. *Exp. Cell Res.* 314:2569–2578. <https://doi.org/10.1016/j.yexcr.2008.05.016>
- Yona, S., K.W. Kim, Y. Wolf, A. Mildner, D. Varol, M. Breker, D. Strauss-Ayali, S. Viukov, M. Guillemins, A. Misharin, et al. 2013. Fate mapping reveals origins and dynamics of monocytes and tissue macrophages under homeostasis. *Immunity.* 38:79–91. <https://doi.org/10.1016/j.immuni.2012.12.001>

Supplemental material

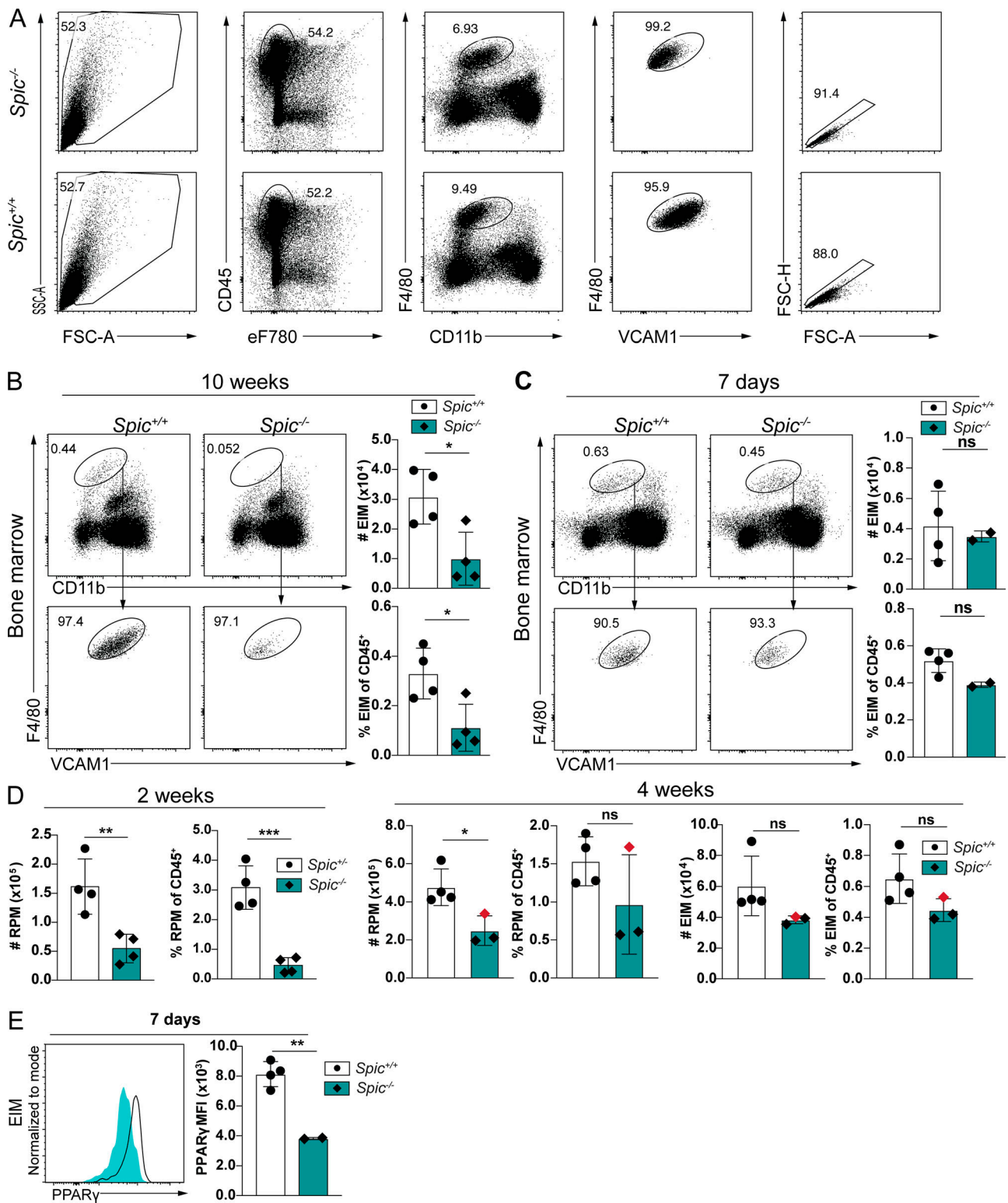


Figure S1. **Gating strategy for identification of RPMs and numbers of RPMs and EIMs in *Spic*^{-/-} and WT mice at different ages.** (A) Gating strategy for identification of RPMs in splenocytes of *Spic*^{+/+} and *Spic*^{-/-} mice harvested at day 7. (B and C) Identification of EIMs by flow cytometry in 10-wk-old (B) and 7-d-old (C) *Spic*^{+/+} and *Spic*^{-/-} mice. Shown are dot plots from representative individuals or groups of mice pregated on live CD45⁺ single cells with adjacent bar graphs showing absolute numbers (top) and percentages (bottom) of EIMs. Symbols represent individual mice. (D) Bar graphs showing absolute numbers and percentages among CD45⁺ RPMs and EIMs in 2-wk-old and 4-wk-old *Spic*^{-/-} mice. (E) Histogram showing PPAR γ expression on F4/80⁺VCAM-1⁺ gated EIMs from a representative individual (left) and adjacent bar graph with values indicating MFI of individuals and mean \pm SD of *Spic*^{+/+} and *Spic*^{-/-} mice. The presented data are representative of two independent experiments. *, P < 0.05; **, P < 0.01; ***, P < 0.001 (unpaired two-tailed Student's t test). FSC, forward scatter.

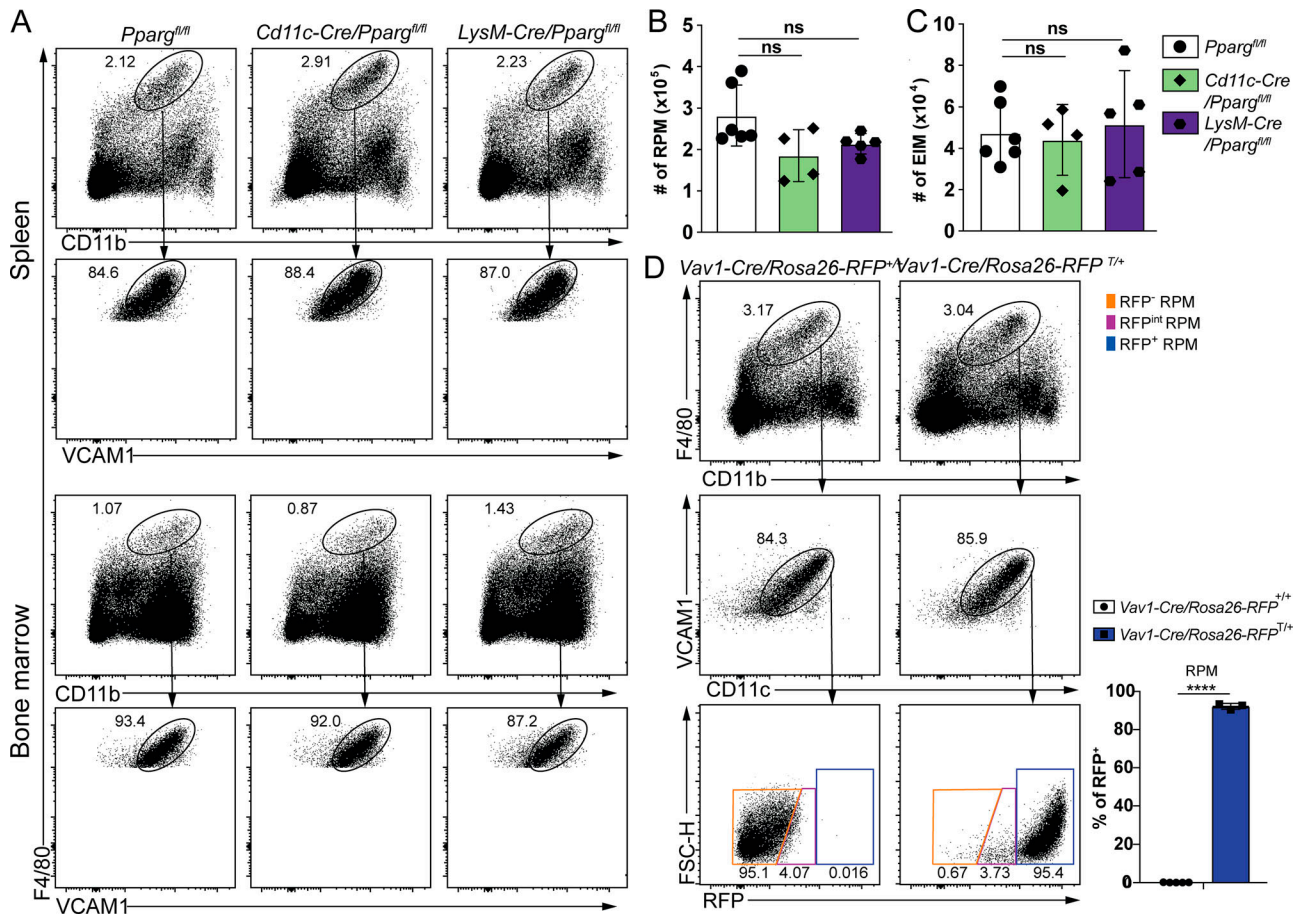


Figure S2. **RPM and EIM numbers in *Cd11c-Cre/Pparg^{fl/fl}* and *LysM-Cre/Pparg^{fl/fl}* mice; Cre activity in RPMs from *Vav1-Cre/Rosa26-RFP* mice.** (A) Flow cytometry of spleen and bone marrow from *Pparg^{fl/fl}*, *Cd11c-Cre/Pparg^{fl/fl}*, and *LysM-Cre/Pparg^{fl/fl}* mice. Gated on live cells. (B and C) Total cell count of RPMs (B) and EIMs (C), gated as in A. (D) Cre activity in RPMs from *Vav1-Cre/Rosa26-RFP* mice. RPMs were gated as depicted on representative flow cytometry plots. Cre activity in RPMs is presented on the bar graph as RFP-positive cells. The presented data are representative of two independent experiments (A and D) or pooled from two independent experiments (B and C; mean and SD of two to three mice per group). No mark, not significant. ****, $P < 0.0001$ (unpaired two-tailed Student's t test). FSC, forward scatter.

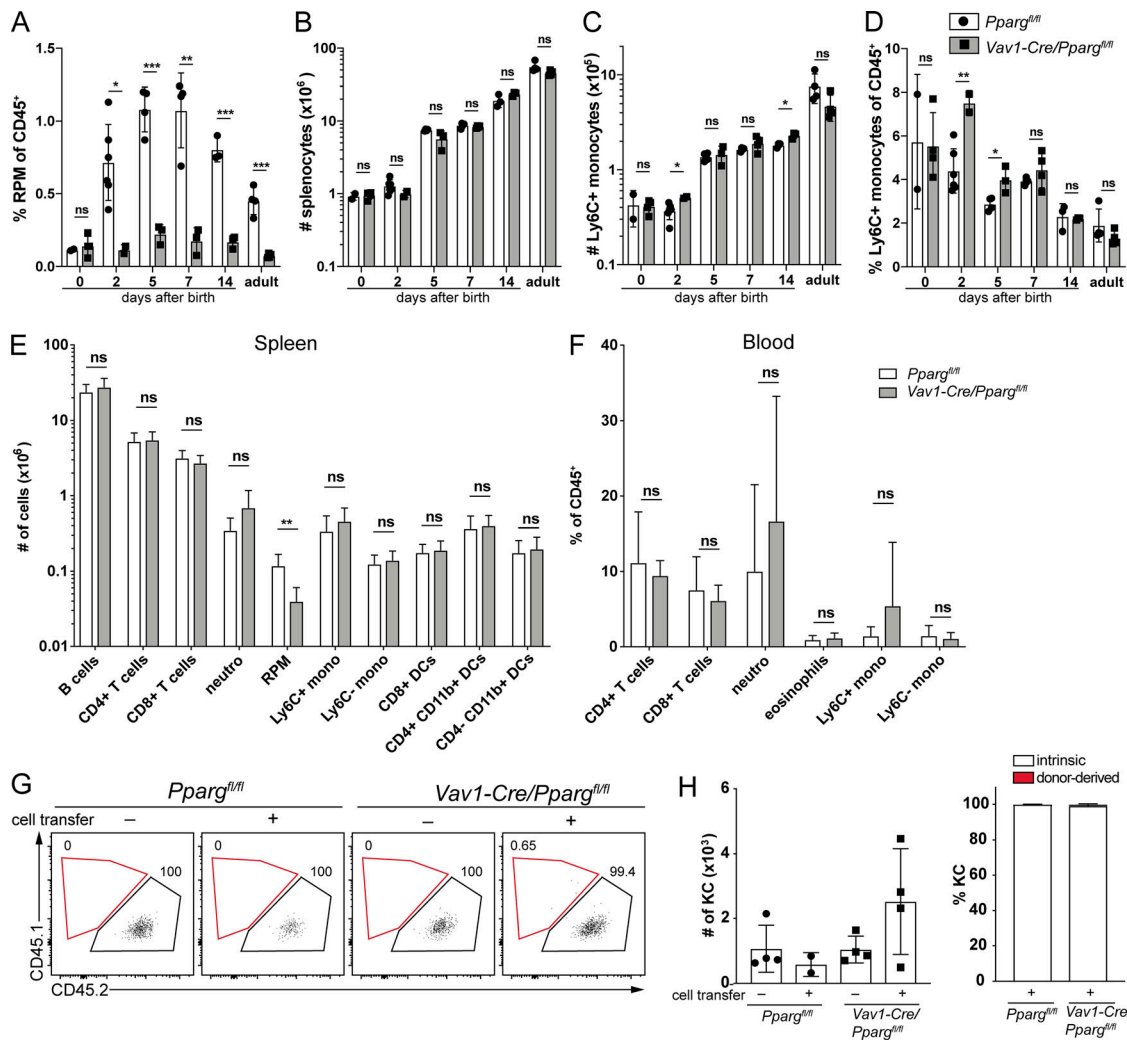


Figure S3. **RPM frequencies and numbers of lymphocyte and myeloid subsets in the spleen of *Vav1-Cre/Pparg^{fl/fl}* mice.** (A) RPM frequencies of CD45⁺ cells at different days after birth. (B) Total cell counts of all splenic cells from *Pparg^{fl/fl}* and *Vav1-Cre/Pparg^{fl/fl}* mice at different days after birth. (C and D) Total Ly6C⁺ monocyte count (C) and frequencies of CD45⁺ (D) at different days after birth. (E and F) Total counts and frequencies of the indicated cell subsets in the spleen (E) and blood (F), respectively, from *Pparg^{fl/fl}* and *Vav1-Cre/Pparg^{fl/fl}* mice at steady state. The indicated subsets were gated as live CD45⁺ cells: CD19⁺ (B cells), TCRβ⁺CD4⁺ and TCRβ⁺CD8⁺ T cells, CD11b^{hi}Ly6G⁺ (neutrophils), SiglecF⁺ (eosinophils), F4/80⁺CD11b^{lo}VCAM-1⁺ (RPMs), MHCII⁺CD11c⁺CD8⁺ (CD8 DCs), MHCII⁺CD11c⁺CD11b⁺ CD4⁺ or CD4⁻ (CD11b DCs), and MHCII⁻CD11c⁻CD11b^{hi}Ly6C⁺ or Ly6C⁻ (monocytes). (G) Dot plots showing KC origin in recipient mice. KCs were gated as live CD11b^{int}F4/80⁺CD64⁺CD11c^{neg}, and the red gates indicate CD45.1⁺ KCs (derived from transferred fetal progenitors). (H) KC counts supplemented with bar graph showing frequencies of donor-derived and intrinsic KCs for transferred mice. The presented data are from a single experiment (A–D, G, and H; mean and SD of two to five mice per group) or representative from three independent experiments (E and F; mean and SD of six mice per group). *, P < 0.05; **, P < 0.01; ***, P < 0.001 (unpaired two-tailed Student's t test).

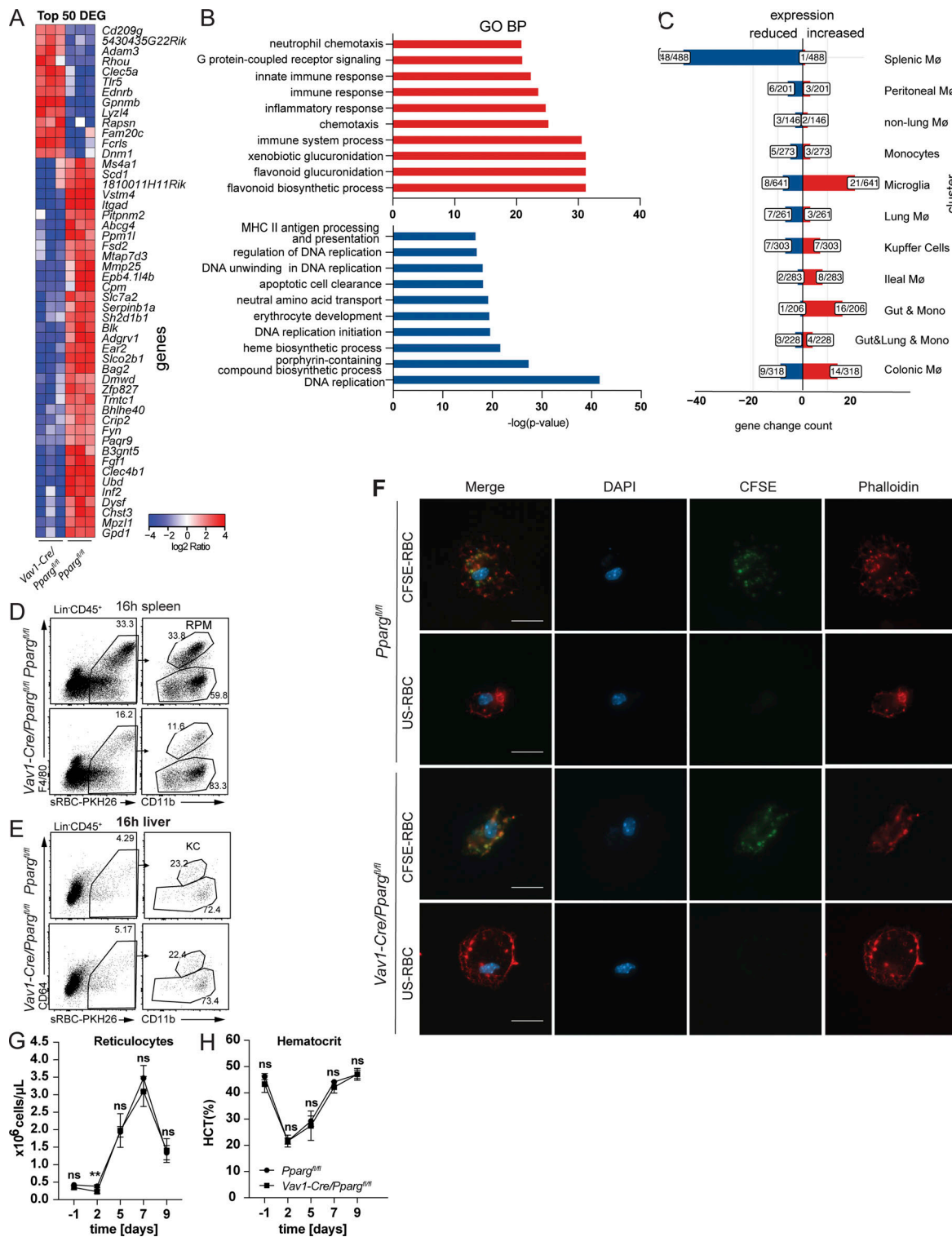


Figure S4. **Differential gene expression in *Pparg*-deficient EIMs; phagocytosis of RBCs and stress erythropoiesis in *Vav1-Cre/Pparg^{fl/fl}* mice.** (A) Heat map showing the top 50 DEGs between *Pparg^{fl/fl}* and *Vav1-Cre/Pparg^{fl/fl}* EIMs (according to absolute values of *gfold*). Cells were isolated from 7-d-old mice. (B) Upregulated (red) and downregulated (blue) GO terms for Biological Process (BP) from comparison of *Vav1-Cre/Pparg^{fl/fl}* over *Pparg^{fl/fl}* EIMs ($P < 0.01$). (C) Bar graphs showing upregulated (red) and downregulated (blue) genes from a comparison of *Vav1-Cre/Pparg^{fl/fl}* over *Pparg^{fl/fl}* EIMs ($|\log_2 \text{ratio}| > 1.5$) within gene signatures of different tissue-resident macrophages (MΦ) and monocytes derived from Lavin et al. (2014). (D and E) Flow cytometry showing the uptake of RBC-PKH26-positive RBCs in the spleen (D) and liver (E) by RPMs and KCs (pregated as Lin⁻CD45⁺) 16 h after injection of PKH26-labeled stressed RBCs. (F) Representative photographs of sorted RPMs from *Pparg^{fl/fl}* and *Vav1-Cre/Pparg^{fl/fl}* mice, which were coincubated for 1 h with CFSE-labeled or unstained (US) lysed RBCs, followed by fixation and phalloidin staining. White scale bars, 20 μm. (G and H) *Pparg^{fl/fl}* and *Vav1-Cre/Pparg^{fl/fl}* mice (8 wk old) were injected i.v. with phenylhydrazine (PHZ; 75 mg/kg) and the count of reticulocytes in the blood (G) and HCT (H) were measured at the days indicated. The presented data are from a single experiment (A–C) or representative of two independent experiments (D–H). **, $P < 0.01$.

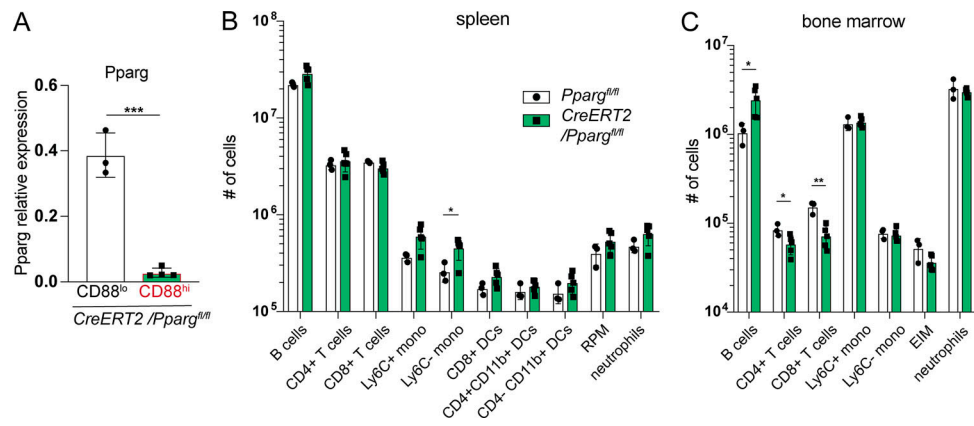


Figure S5. **Spleen and bone marrow cellularity after conditional depletion of *Pparg* in adults.** (A) *Pparg* expression determined by RT-PCR in RPMs derived from CD88^{lo} and CD88^{hi} from *CreERT2/Pparg^{fl/fl}* mice treated with tamoxifen. The values are normalized to a house-keeping gene (*G6PD*X). (B and C) Cell counts of indicated populations in *Pparg^{fl/fl}* and *CreERT2/Pparg^{fl/fl}* mice in the spleen (B) and the bone marrow (BM; C). The presented data are representative of three independent experiments (A–C; mean and SD from three to five mice per group). *, $P < 0.05$; **, $P < 0.01$; ***, $P < 0.001$ (unpaired two-tailed Student's *t* test).